T.R.
BOLU ABANT İZZET BAYSAL UNIVERSITY
INSTITUTE OF GRADUATE STUDIES
Department of Physics

EFFECTS OF WIRE DIAMETER, TAPE THICKNESS, AND ROLLING RATIO ON THE SUPERCONDUCTING PROPERTIES OF MONOCORE Fe/MgB_2 CONDUCTORS

MASTER OF SCIENCE

QAYS MAATH AHMED

ACADEMIC SUPERVISOR
PROF. DR. IBRAHIM BELENLI

BOLU, DECEMBER - 2023

APPROVAL OF THE THESIS

Effects of Wire Diameter, Tape Thickness, and Rolling Ratio on the Superconducting Properties of Monocore Fe/MgB_2 Conductors submitted by **Qays MAATH AHMED** and defended before the Examining Committe Members listed below in partial fulfillment of the requirements for the degree of **Master of Science** in **Department of Physics, Institute of Graduate Studies of Bolu Abant Izzet Baysal University in 5.12.2023** by

Examining Committee Members	**Signature**
Supervisor Prof. Dr. İbrahim BELENLİ Bolu Abant İzzet Baysal University	....
Member Prof. Dr. Hakan YETİŞ Bolu Abant İzzet Baysal University	....
Member Prof. Dr. Özgür ÖZTÜRK Kastamonu University	....

Prof. Dr. İbrahim KÜRTÜL

Director of Instıtute of Graduate Studies

ETHICAL DECLARATION

In this thesis dissertation that was properly prepared according to the Thesis Writing Rules of Bolu Abant İzzet Baysal University of the Institute of Graduates Studies, I hereby declare that;

- All data, information, and documents presented in the thesis were obtained in accordance with the academic and ethical rules,
- All data, documents, assessments, and results were presented in accordance with the scientific ethical and moral rules,
- All works that were benefitted in the thesis were appropriately cited,
- No alteration was made in the data used,
- Study presented in this thesis is original,

Otherwise, I declare that I accept the loss of all my rights in case any contradiction that may arise against me.

The similarity rate obtained by using the Turnitin program, a plagiarism detection software, is within the limits approved by the University Senate.

____

QAYS MAATH AHMED

ABSTRACT

EFFECTS OF WIRE DIAMETER, TAPE THICKNESS, AND ROLLING RATIO ON THE SUPERCONDUCTING PROPERTIES OF MONOCORE Fe/MgB_2 CONDUCTORS
MSC THESIS
QAYS MAATH AHMED
BOLU ABANT IZZET BAYSAL UNIVERSITY
INSTITUTE OF GRADUATE STUDIES
DEPARTMENT OF PHYSICS
(SUPERVISOR: PROF. DR. İBRAHİM BELENLİ)

BOLU, DECEMBER 2023
(xiv + 64)

In this work, we studied the superconducting properties of MgB_2 monocore iron sheathed wires of different diameters and tapes of different thicknesses produced using the in-situ powder-in-tube (PIT) method. We manufactured wires and tapes using the in-situ PIT method by filling the iron tube with previously prepared unreacted Mg and 2B powder. Thus, the 15 mm diameter tube underwent a groove rolling process to reduce its diameter to 3 mm to produce wires. In addition, the wires were subjected to cold drawing and were cut with diameters of 2.5 mm, 2.0 mm, 1.7 mm, and 1.3 mm. Therefore, these wires with different diameters were subjected to a flat rolling process to produce tapes, and parts of the tape sample were cut with different thicknesses of 1.2 mm, 0.9 mm, 0.6 mm, and 0.4 mm. During these processes, the wires and tapes were subjected to intermediate heat treatments at a temperature lower than the synthesis temperature of MgB_2 to reduce the mechanical stress due to these processes. After these steps, heat treatment was carried out at 700°C for 2 hours using a tube furnace. We have examined the effects of electrical / superconductivity for all samples. Temperature-resistance and current-voltage measurements were made using a cryostat system at magnetic fields of up to 7 Tesla by cutting samples with a length of 25 mm from the middle part of our samples. The results indicate that the tape sample that is 1.2mm thick is flat rolled from wire with diameters of 2.0mm and possesses the most suitable properties for superconducting than the tape samples due to its higher T_c at 37.76K. The most important result is that the wire sample with a diameter of 1.7mm shows the highest T_c among the wire and tape samples at 37.87K. On the other hand, Tapes of smaller thickness show faster degradation of J_e, which makes them less suitable for applications involving strong magnetic fields.

KEYWORDS: Superconductivity, PIT, MgB_2/Fe, Monocore, Wire, Tape

ÖZET

TEL ÇAPI, ŞERİT KALINLIĞI VE HADDELEME ORANININ TEK DAMARLI Fe/MgB_2 İLETKENLERİN SÜPERİLETKENLİK ÖZELLİKLERİ ÜZERİNDEKİ ETKİLERİ
YÜKSEK LİSANS TEZİ
QAYS MAATH AHMED
BOLU ABANT İZZET BAYSAL ÜNİVERSİTESİ
LİSANSÜSTÜ EĞİTİM ENSTİTÜSÜ
FİZİK ANABİLİM DALI

(TEZ DANIŞMANI: PROF. DR. İBRAHİM BELENLİ)

BOLU, ARALIK - 2023
(xiv + 64)

Bu çalışmada, in situ boru içinde toz (BİT) yöntemi kullanılarak üretilen farklı çaplarda MgB_2 tek damarlı demir kılıflı teller ve farklı kalınlıkta şeritlerin süperiletkenlik özelliklerini inceledik. Önceden hazırlanmış reaksiyona girmemiş Mg ve 2B toz karışımını demir boruya doldurarak PIT yöntemiyle tel ve şerit ürettik. Bu toz ile doldurulmuş 15 mm çapındaki demir boruyu uzatarak 3 mm çapında tel haline getirmek için bir oluklu haddeleme cihazı kullanıldı. Daha sonra bu tele soğuk çekme uygulanmış ve kademeli olarak 2,5mm, 2,0mm, 1,7mm ve 1,3mm çaplarında tel örnekler elde edilmiştir. Bu nedenle, bu farklı çaplardaki tellerden şerit örnekler üretmek için düz haddeleme işlemi uygulanmıştır. Farkı çaplardaki tellerden düz haddeleme işlemi ile 1,2mm, 0,9mm, 0,6mm ve 0,4mm farklı kalınlıklarında şerit formunda örnekler elde edilmiştir. Bu işlemler sırasında teller ve şeritlerde mekanik deformasyon nedeniyle oluşan gerilmeleri azaltmak için MgB_2'nin sentez sıcaklığından daha düşük bir sıcaklıkta ara ısıl işlemler uygulandı. Bu adımlardan sonra 700°C'de 2 saat süreyle boru fırın içerisinde argon basıncı altında ısıl işlem uygulandı. Tüm örneklerin elektriksel/süperiletkenlik özelliklerini inceledik. Sinterlenen örneklerin orta kısmından 25 mm uzunluğunda numuneler kesilerek 7 Tesla'ya kadar manyetik alanlarda bir kriyojenik soğutma sistemi kullanılarak sıcaklık-direnç ve akım-gerilim ölçümleri gerçekleştirildi. Sonuçlar, 2.0mm çapında telden düz haddelenmiş ve daha yüksek T_c'ye 37.76K' sahip olduğundan şerit örneklerden daha uygun süperiletken özelliklere sahip 1.2mm kalınlığındaki bant numunesinin tel numunelerine göre en uygun özelliklere sahip olduğunu göstermektedir. En önemli sonuç, tel ve şerit örnekler arasında en yüksek T_c'yi 37.87K'de gösteren tel numunesinin 1.7mm çapında olmasıdır. Öte yandan, daha küçük kalınlığa sahip şeritlerde J_e daha hızlı bozulma göstererek bunları güçlü manyetik alanları içeren uygulamalar için daha az uygun hale getirmektedir.

ANAHTAR KELİMELER: Süperiletkenlik, TİT, MgB_2/Fe, Tek damarlı, Tel, Şerit

TABLE OF CONTENTS

Page

LIST OF FIGURES

Page

LIST OF TABLES

Page

LIST OF PICTURES

Page

LIST OF ABBREVIATIONS AND SYMBOLS

PIT	: Powder In Tube
PeIT	: Pellet In Tube
CTFF	: Continuous Tube Filling and Forming
CHPD	: Cold High Pressure Densification
HIP	: High Isostatic Pressure
HTS	: High-temperature superconductors
IMD	: Internal Magnesium Diffusion
LIMD	: localized Internal Magnesium Diffusion
CNTs	: Carbon nano-tubes
YBCO	: Yittrium Barium Copper Oxide
BSCCO	: Bismuth Strontium Calcium Copper Oxide
XRD	: X-Ray Diffraction
SEM	: Scanning Electron Microscopy
MRI	: Magnetic Resonance Imaging
SQUID	: Superconducting quantum interference devices
HP	: Heat Process
$T_{c\ offset}$	: Offset superconducting transition temperature
$T_{c\ onset}$	: Onset superconducting transition temperature

ACKNOWLEDGEMENTS

I would like to express my sincere gratitude to my supervisor, Prof. Dr. Ibrahim Belenli, for his guidance, motivating suggestions, and support throughout the research period and completion of this thesis.

I am deeply grateful to Prof. Dr. Hakan Yetiş for his insightful comments, and constructive suggestions.

I also extend my sincerest thanks to Dr. Fırat Karaboğa and PhD student Doğan Avci for their availability whenever I needed during the experimental phase of my research.

Finally, I am deeply indebted to my family for their unwavering support, constant motivation, and endless patience throughout my studies. Their love and encouragement were a source of strength throughout this challenging journey.

1. INTRODUCTION

Some materials known as superconductors have the ability to conduct electric current with a zero resistance below its certain critical temperature T_c. Superconductivity phenomena were discovered in 1911 by Kammerlingh Onnes pure Hg at T=4.2 K (1). Therefore, this important discovery which has opened the door to new ambitions for applications in an efficient magnet and energy technology, triggered plenty of scientific interest.

Energy demand in the modern world of the 21^{st} century has been suddenly rising up with the population rate growth and human consumption toward scarcity of resources. That is why many researchers have been highly worked to find suitable new energy resources and solutions; at the same time, efficient use of existing energy sources become more important. One of the most convenient solutions is the use of superconducting power wires, which superior the electrical current without any losses of heat and energy. In future, superconductors will replace most of the power transmission lines and technologies. Magnesium diboride MgB_2 superconductors have much better properties such as high critical current density J_c, simple good chemistry in the form of AX_2, simple internal crystal structural, low mass density, which is equal to 2.56 g/cm^3, low anisotropy, and high upper critical magnetic field strength B_{c2} (2).

Within the realm of intermetallic superconductors, magnesium diboride MgB_2 reigns supreme, boasting the highest critical temperature T_c (3), and it does not have a serious weak link problem at grain boundaries. MgB_2 samples are fabricated in various formations as wires, tapes, thin films, single crystals and bulk samples (4). Many major critical parameters of MgB_2 wire were improved to investigate more efficiency and quality by alternative techniques and processes. All these distinguished efforts are looking forward to improving the current density (J_c) upper the magnetic field (B_{c2}) in order to use it in superconductor applications and technologies. To produce this type of superconductor in the case of MgB_2, it may be possible to use either an in-situ or ex-situ technique, where the in-situ technique is considered to have better efficiency than the ex-situ which is necessary for improving the wires/tapes properties. Generally, the in-situ processed MgB_2 wire has an extremely porous core structure which decreases the (J_c), and that is expressed as a disadvantage literally (5).

In this case, the production of MgB_2 porosity is due to the resulting volume contraction and sizes of compositions from the chemical reaction of the magnesium-boron (6). The current carrying properties of the MgB_2 wires during the in-situ wire/tapes are a matter that needs to be improved. Some alternative ideas have been enhanced in improvements upon the densification of the MgB_2 wire core due to the chemical interaction which was reported (7,8). Otherwise, there is another method that is used in the heat treatment process under hot iso-static gas pressure in terms of porosity problem, which is called a hot iso-static pressure (HIP) method. This technique is used in-situ MgB_2 wires made using unreacted Mg+2B precursor. Consequently, the HIP method is applied on a small piece of the superconductor wire, and the wire roundness will be adversely affected especially when applying high pressure during the solid state phase. Therefore, using the HIP method in heat treatment of the multi-filamentary wires depending on the sheath material and geometry, some structural problems appear (9).

Giunchi et al. improve the reactive liquid magnesium infiltration technique, and this is considered to have another method of the powder into tube (PIT) method (10). A magnesium rod (Mg) is positioned in the central region of the Nb composite tube, and boron powder (B) is filled around the Mg rod. Fine grains and compact magnesium diboride layer are found at the core/sheath boundary region in this method.

The development of the infiltration method and fabrication of MgB_2 wire with a critical current density ($T \approx 4.1K$, $B \approx 8T$) of more than $10^5 Amp/cm^2$ by internal magnesium diffusion technique (IMD), which improved the wire performance by Hur et al. with using of nano silicon carbonate SiC addition during a low annealing temperature treatment process (11). In the internal magnesium diffusion technique IMD wire, we can obtain a maximum J_c, but the core of the wire leaves an empty hole region at the centre because of the diffusion of magnesium (Mg) rod towards the surrounding boron (B) powder. These central empty holes constitute a main disadvantage for scaling up the IMD wire and decrease J_c as the overall cross-section area of the IMD wire is reported (12). Maeda et al. used the localized internal magnesium diffusion (LIMD) technique, which replaced the traditional magnesium rod with coarse-grained magnesium powder and was connected together with the cold high-pressure densification (CHPD) technique (13). Utilizing crystalline boron powder with LIMD and CHPD techniques led to the production of long MgB_2 wires, which are low-cost, and economical than the IMD wires. A high J_c of $10^4 A/cm^2$ at $T \approx 4.2K$ and applying magnetic strength up to 8T was investigated for this cost-effective wire fabrication. While LIMD combined with CHPD did not fully resolve the issue of porosity, it could demonstrably increase the density in the core region by effectively reducing the initially existing void spaces, and these commonly arise from the inadequate compression in the conventional powder-in-tube (PIT) technique. Low core density poses a significant challenge to reaching high J_c values, especially in the case of in-situ MgB_2 wires. Generally, amount of porosity is determined by the fabrication of in-situ MgB_2 wires and high-performance wires can be achieved by increasing the capacity of superconducting regions, which contributes to the grain connectivity to improve critical current density J_c. External additives incorporated during in-situ MgB_2 wire production further elevate the critical current density, particularly at high and maximum magnetic field values (14,15).

Many previous studies have reported that are several types of carbon-based additives; for instance, carbon nano-tubes CNTs, nano-silicon carbonate SiC, or other nano-carbons are sufficient solutions to increase the J_c in high field strengths, their efficacy in improving J_c at elevated magnetic field values remains insufficient (16). Low values of J_c are sufficient in terms of low magnetic field applications of MgB_2 wires, for example, low-field magnetic resonance imaging MRI (17,18). The sintering process and substituting the carbon technique with boron make modifications by the enclosed flux mechanism in MgB_2. In addition, silicon carbonate addition significantly enhances the critical current density J_c and critical magnetic field B_{c2}. Therefore, the formation of nanocarbon agglomerates presents a significant obstacle to the large-scale fabrication of wires. MgB_2 wire fabrication primarily relies on malic acid ($C_4H_6O_5$) as its source of carbon. Homogeneous carbon incorporation is achieved in this organic compound through the wet mixing process. Employing malic acid allows us to understand the formation of carbon and how it is enveloped by boron, preventing agglomeration during the reaction. The properties of using in-situ MgB_2 wires can be developed in a big scale of magnetic field values by the inclusion of malice acid (16,19). There are many factors that determine the critical current density of in-situ MgB_2 wires; one of these factors and parameters is the formation of some oxidations, for instance, as magnesium oxides in between the superconducting MgB_2 grains since magnesium particles are easily oxidized (20). These insulating barriers of magnesium oxides may create boundaries and spaces in the presence of oxygen and can highly inhibit the flow of current such as J_c; this is called the percolation threshold, which is caused a connectivity problem in the MgB_2 core internal structure (6).

Otherwise, the oxygen-rich boron phases were found, such as formulas of MgO, BO_x, etc., with different sizes depending on the coherence length, have the potential to act as the effective pinning centres and improve the critical current density J_c under the influence of an external magnetic field (16). The formation of small-sized BO_x exhibits the pinning of the flux at intergranular regions and areas, and increase in oxygen content appears to cause large magnesium oxide layers and these barriers restrict the number of available current paths, which reduces the path probability for resistanceless current. The well-interconnected grains have a certain role in increases of the critical current density J_c due to the limited pathways for current flow often found from excess oxide formations. Stoichiometry of magnesium diboride is so necessary in terms of the dominance and controller phases or decreases of oxidation-rich secondary phases. Specifically, the magnesium oxide phase preferentially occupies the intergranular regions (21).

Many researchers and reports explained the Mg wire samples and showed that the superior critical current density J_c may be improved as a ratio up to (10 %) excess-Mg. On the other hand, the studies also showed that Bc_2 and B_{irr} (irreversible) of MgB_2 wires were exhibited when excess magnesium was included (17).

Consequently, the properties of the MgB_2 superconductor often existed to be heavily reliant upon the temperature treatment for the excess-Mg wires. There were many studies have been shown to achieve the impact of the Mg/B ratio on the properties of MgB_2 samples, but there is no consensus due to the fact that the differences between the results of previous studies reveal the impacts of Mg nonstoichiometry on the MgB_2 superconductivity performance that are present (22,23).

At high magnetic field values, the Mg deficient samples showed better critical current densities compared with that of the magnesium excess samples. It was findings from previous research indicate that a lack of magnesium, even at ratios close to 1%, exhibits the J_c when applied to a magnetic field. There are possible variations in superconducting properties and internal structure because the magnesium nonstoichiometry results from the magnesium particle sizes and purities, mixture homogeneity and changeability in the magnesium oxides MgO formation. Consequently, it is highly necessary to make improvements to the superior properties of magnesium diboride MgB_2 wires with Mg/B improvements (18). The use of in-situ technique helps to improve the performance of MgB_2 wires and tapes under applying an external magnetic field and enhance their critical current density when pellet-in-tube technique is used (24).

In this study, we have studied the fabrication of the Fe/MgB_2 wires and tapes and carried out cryogenic measurements for their conductivity characterizations and determination of the superconducting properties.

This thesis is arranged as follows: Chapter 2 introduces the aims and the main objectives, which reveals the major idea of this thesis. Chapter 3 talks deeply about the theories and superconductivity background in detail. For instance, the differences between type I and type II superconductors individual and their critical properties and factors are based on the important theories and hypotheses that belong to the superconductivity phenomena. Chapter 4 describes the fabrications, methods for preparing MgB_2 wires and tapes, and techniques. Therefore, we are looking deeply at the fundamental properties of the MgB_2 superconductor, its internal crystal structural and electronic behaviour, and the basic distinctions of superconducting. Chapter 5 explains experimentally how to make preparation and productions for MgB_2 superconductor wire and tapes into many methods and techniques during tests and measurements. Chapter 6 includes experimental results and discussion. In Chapter 7, conclusions are presented, and the results are interpreted as individual structural and superior characterization measurements and conductivity properties. Otherwise, some important results of and recommendations of this study are concluded. Chapter 8 it's considered as a list of the whole references which are used in this research.

2. AIM AND SCOPE OF THE STUDY

This study is looking forward to producing Monocore MgB_2/Fe wires and tapes with the best engineering shape in terms of superconducting properties, which are manufactured in-situ using the powder-in-tube method (PIT) and measure the electrical and mechanical properties of these wires and tapes at different magnetic fields between (0-7 T).

The Monocore MgB_2/Fe wire and tapes will be produced in different dimensions. The wire and tape samples will be produced using groove rolling, cold drawing, and flat rolling techniques. Round wires will be produced as the first step. The round wires will be used for the production of tapes in various thicknesses via flat rolling. Necessary heat treatment recipes will be applied to tape samples under controlled conditions. Therefore, the electrical measurements will be carried out to obtain the current-voltage (I-V) and resistance–temperature (R-T) behaviours of the samples. Finally, the morphology and structure of the sample will be examined.

3. THEORY AND BACKGROUND

3.1 Superconductivity

In 1908, a Dutch scientist who was called Heike Kamerlingh Onnes of Leiden University successfully liquefied helium from a gas into liquid; it had been considered the last un-liquefied gas in the world. In that meantime, scientists already had the basic knowledge that the resistance of some pure metals drops down when the temperature decreases to very low temperatures, where zero resistance is achieved below its critical temperature. Liquefied helium was highly provided the lowest temperature of 4.2 K at that time. Many metals were used by using liquefied helium to understand what was the behavior between resistance and temperature. In 1911, Onnes cooled a sample of mercury Hg by liquefied helium; he found and noticed spectacularly that the resistance of mercury dropped to zero at about 4.2 K (−269.2°C), and this temperature was called the critical temperature of mercury. This phenomenon, known as superconductivity, depends on three important parameters: temperature, current density, and magnetic field strength are represented in a 3-D sketch of the critical surface of MgB_2, NbTi, and Nb_3Sn superconductors (1).

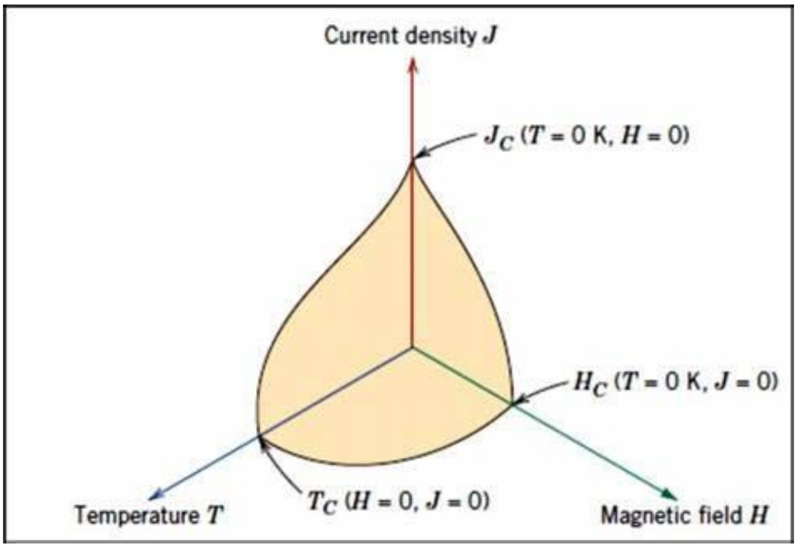

Figure 3.1. 3-D sketch of critical surface of superconductors.

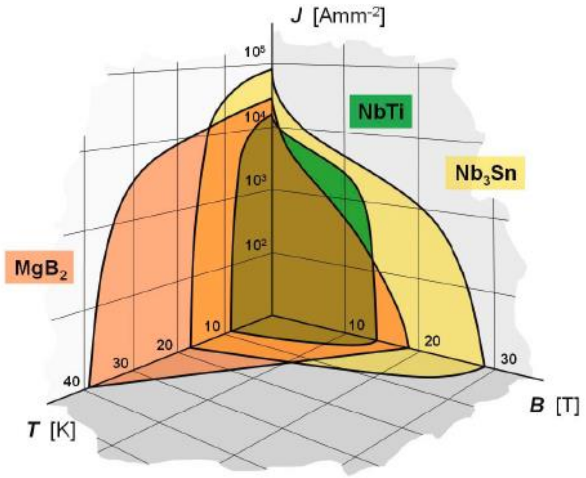

Figure 3.2. critical surfaces of MgB_2, NbTi and Nb_3Sn (25).

Any element, metallic alloy, or compound that has the ability to conduct electricity without resistance below a certain temperature is called a superconductor. Superconductors also exhibit a unique property called the Meissner effect, the expulsion of a magnetic field from the interior of a superconductor when it is cooled below its transition temperature. Energy is lost and dissipated when a superconductor is subjected to an alternating current AC or an alternating magnetic field, but quite the opposite when a direct current DC is passed through (26). Superconductors are subdivided into low-temperature superconductors (LTS), which can be used nearly the boiling point of He (T=4.2K), and high-temperature superconductors (HTS), which can be operated above the nitrogen boiling point of T=77K. Low and high-temperature superconductor materials were discovered in 1911 and 1987, respectively. The phenomenon of superconductivity has appeared at very low temperatures, which needs to cool system for running in order to decrease temperature. Therefore, high-temperature superconductors (HTS) are preferred for use in power applications as this reduces the energy dissipated in the cryogenic system.

3.1.1 Discovery of Superconductivity

The materials are lost their electrical resistance completely versus currents when the temperature is under critical temperatures. These materials are called superconductors materials, and this phenomenon is called superconductivity, which was discovered in 1908 by a Dutch physicist called Onnes. In 1911, he analyzed various resistance of metals at low temperatures by using liquefy helium (T_{boil}=4.2K). Onnes found out that the resistance of mercury was very close to zero at 4.2K and considered it a superconductor. After that, Onnes observed many metals whose resistance went to zero below a certain critical temperature T_c for each, he tried to observe many metals by using liquid helium at low temperatures, and due to the analyzing processes, he got the Nobel Physics Prize in 1913 (1).

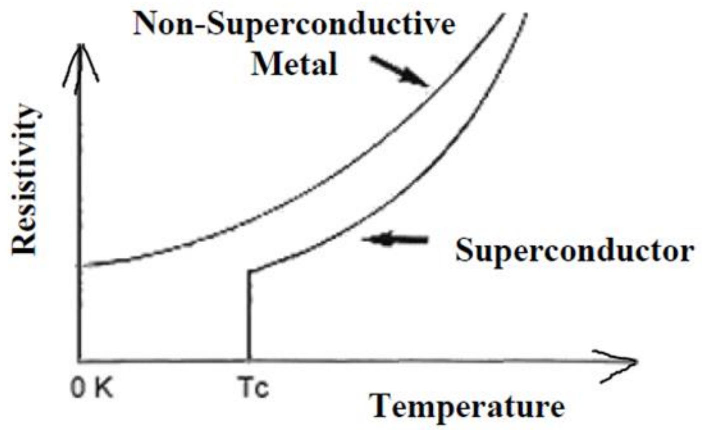

Figure 3.3. Critical temperature of resistivity of superconductor metal and non-superconductive.

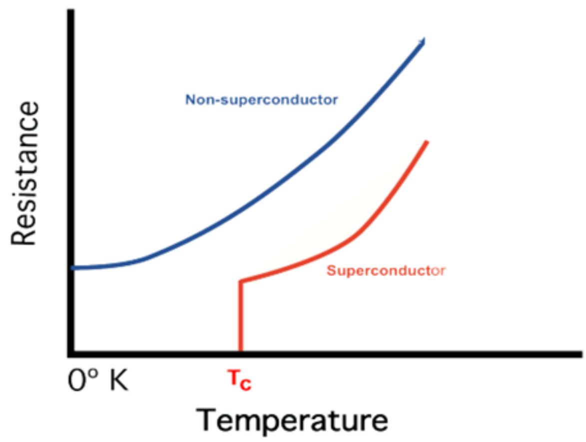

Figure 3.4. Temperature dependence of resistance in a metal and a superconductor.

The discovery of superconductivity was a very important event that made many scientific discoveries possible, including the discovery of high-temperature superconductors (HTS) and many other superconducting materials. Scientists have investigated many copper-oxygen containing compounds in the search for new superconductors. In 1990, Bi2223 and YBCO materials had come close to commercial manufacturing due to their high efficiency in magnetic fields and the possibility of their environmentally friendly production (27,28).

3.1.2 Zero resistivity

Superconducting material has zero resistivity below its critical temperature (T_c), or called the transition temperature, it loses its resistance completely against the electric current flows through its body. Zero resistivity is achieved suddenly in superconductors when their temperature becomes equal to or lower than the transition temperature (T_c). When the temperature of a superconducting material goes below its critical temperature it will display extraordinary behaviour in terms of electrical and magnetic properties.

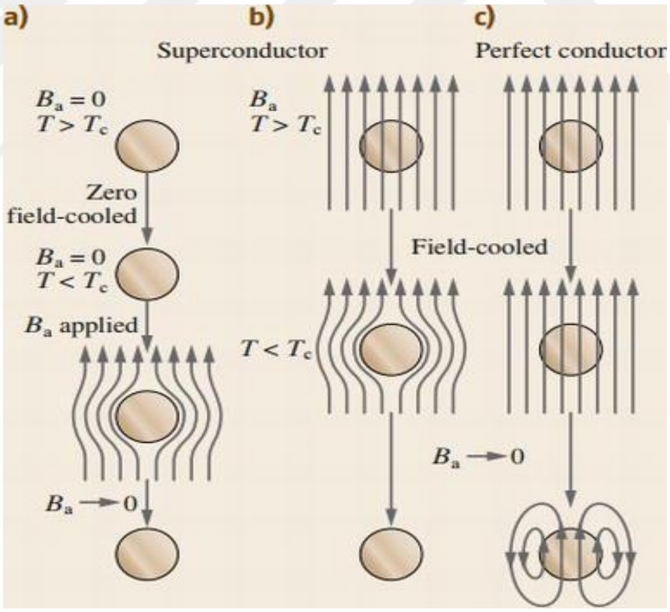

Figure 3.5. (a) The magnetic flux is excluded from the interior of a superconductor, (b) in the presence and absence of field-cooling, (c) in contrast, a field-cooled perfect conductor shows presence of interior magnetic flux.

As shown in Figure 3.5, it represents the differences between a perfect conductor and a superconductor, respectively. That is, the superconducting materials expel all magnetic field when it becomes below the transition temperature

(T_c). In this case, the magnetic field cannot penetrate and goes inside this material in all circumstances since the magnetic flux vanishes inside a sample when $T < T_c$ and switches into a perfect diamagnetism because of the Meissner effect (29).

3.1.3 Meissner Effect

In 1933, miessner and ochsenfeld observed that the superconductor materials repel the magnetic fields under T_c. They analyzed the superconductor's characteristics, in particular the transition from normal state to superconducting state, and found out why superconductors behavior do like that. This effect was defined as meissner effect (30).

The Miessner effect occurs when a magnetic field penetrates the superconductor material, which generates currents within a very thin surface layer of thickness λL. This current creates a magnetization M which causes the interior and leads to be $4\pi M+H=0$ (31). Therefore, current expels the applied magnetic field out of the superconductors materials, which means $B_{Inside}=0$, the behavior of this case will be as perfectly diamagnetism with a magnetic susceptibility $\chi = -1$ as long as it is under an applied magnetic field below B_c. Since the resistivity almost equals zero and super current flows continuously without losing energy in the form of heat (32).

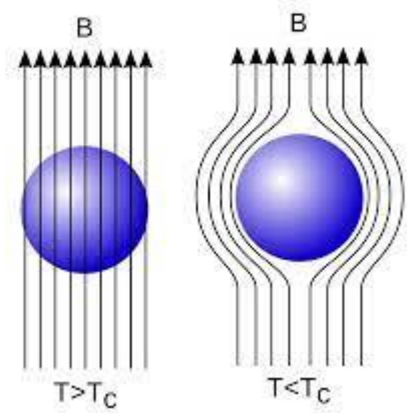

Figure 3.6. Meissner effect.

Figure 3.7 represents the critical temperature against the critical magnetic field and also shows the superconducting and normal states related to type I superconductors. When the magnetic field strength is raised above a critical $B_c(T)$

point, superconductor materials lose their superconducting properties and switch to a normal state. Therefore, the critical magnetic field depends on temperature:

$$B_c\,(T) = B_{c0}\,[1- (T / T_c)]$$

In the previous relation, B_{c0} means the value of the magnetic field at T=0K, and T_c is the critical temperature or transition temperature between normal and superconductor states (33). In 1935, the two brothers Heinz and Fritz London tried to improve the superconductivity theory of electrodynamics.

Consequently, by using their equation which is called the London equation, they found that when going inside the superconductive surface gradually, the magnetic field reduces exponentially. The magnetic field is generated from currents that occur on superconductive outer surface penetrates to a certain degree, and the expression of the decay length of this formation is known as London penetration depth (λ). Penetration depth means that the maximum penetration possible it's given by the following formula (34):

$$B(x) = B_0 \exp\,(-x/\lambda)$$

Where is x: the distance from the superconducting material surface.

λ: The penetration depth.

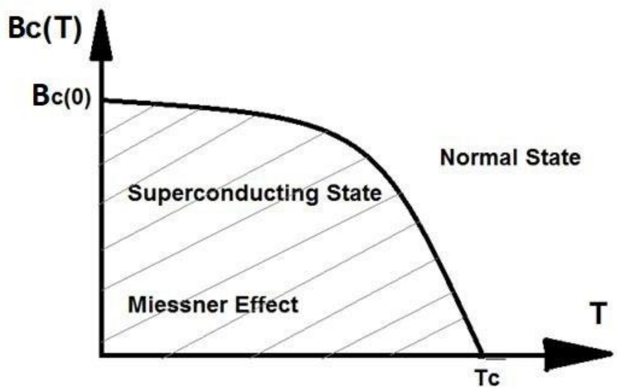

Figure 3.7. Critical temperature dependence and critical magnetic field representation.

In 1950, Ginzburg and Landau advanced an explanation theoretically that is called the Ginzburg – Landau theory, interested in the symmetrical characteristics of superconductors. This theory explains the superconductive microscopic characteristics, although it is considered insufficient for microscope characteristic description (35).

In 1957, John Bardeen, Leon Cooper, and John Robert Shcrieffer from the University of Illinois. These three physicists put the first step in understanding superconductivity and advanced a sufficient description of microscope superconductor characteristics which is known as BCS theory. This theory explains how the electrons flow going in regular movement, not randomly, and it is dominated by the vibrations of a structural lattice of superconductors. Below the transition temperature T_c, collisions disappear while electrons are moving without any resistance inside the crystal structure. When an electron passes near an ion, it pulls towards itself since the other electron takes the same speed under attraction force among the two elections as couples and pulls each other indirectly, this is known as Cooper's pairs, and this theory plays an important role on understanding the microscope characteristic of superconductivity (33).

The BCS theory plays an important role in explaining the mechanism of superconducting materials in very low temperatures with an estimation of 30 K as the highest T_c value and tries to advance a convincing explanation. Otherwise, this BCS theory is unable to put an explanation in the case of using HTS materials in many high-temperature T_c values. Therefore, the critical temperature of 39 K for MgB_2 is considered high so it is difficult for the BCS theory to explain it accurately (36).

3.1.4 Type I and Type II Superconductors

In 1957, Alexei Abrikosov studied the characteristics of the metalic superconductors in the presence of an applied magnetic field and analyzed their performance. Hence, he classified superconducting materials as Types I and Type II. Type I superconducting materials such as Al, Hg, and Sn are characterized as diamagnetic and soft, and magnetization raises up till it reaches the critical magnetic field H_c and goes to zero at that value suddenly at that temperature. These Type I superconducting metals show meissner effect when the applied magnetic field is under the critical magnetic field (37).

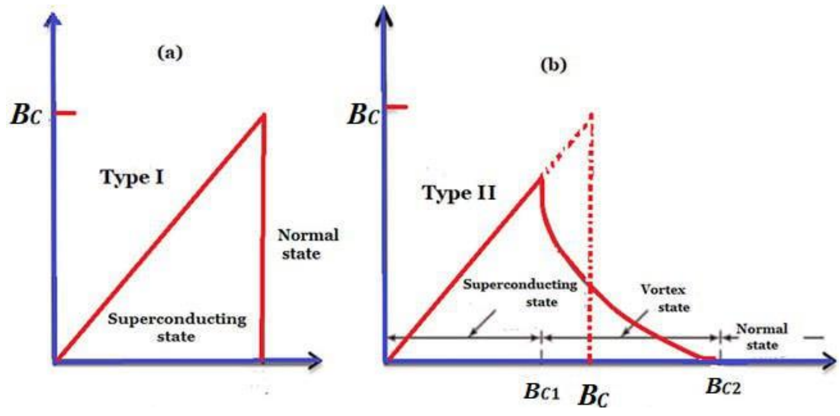

Figure 3.8. The behaviour of type I and type II superconductors under magnetic field.

In Figure 3.8, it's clear that Type II superconductors are determined by B_{c1} and B_{c2}, as shown. In the case of an applied magnetic field that is less than B_{c1}, the performance of these materials expel the magnetic field and behave the same as a Type I superconducting material. Otherwise, if the applied magnetic field is between B_{c1} and B_{c2}, the material is found in a vortex state or a mixed state. When a material undergoes a mixed or a vortex state, it can have zero resistance, and the flux penetrates gradually and partially since if the sample passes or reaches the upper critical field B_{c2}, it will transition to the normal state immediately. Current is carried into the Type II superconducting materials that lead to creating the Lorentz force, which is faced by the magnetic flux while the Lorentz force tries to expel the field outwards. If it cannot, heat is produced because the magnetic flux lines cannot be completely discarded. Also, this causes the superconductors to warm and the critical temperature of the T_c point to fall. It may be achieved to reach zero resistance by adding impurities and doping process (38).

3.1.5 High-temperature superconductors

Much research has been conducted for years to improve new superconducting materials at higher temperatures. For instance, niobium germanium (Nb_3Ge) is known to have a critical temperature of T=23.2K. In 1986, Karl Alex Müller and J. Georg Bednorz made a new important step in the discovery of superconducting materials when they found that ceramic superconductors made of barium, lanthanum, copper, and oxygen could superconduct at around 35K (39). Other researchers showed that the formula of superconducting lanthanum-barium copper oxide is $La_{2-x}Ba_xCuO_4$, where x is typically between 0.05 and 0.15. Additionally, some researchers found that using strontium instead of barium results in a transition temperature of 36K. Research on high-temperature superconductivity began in 1986, and superconductivity was observed in compounds involving copper, barium, yttrium, and oxygen approaching 92K in 1987 by research groups from the Universities of Houston and Alabama (28). Maeda and his group synthesized $Bi_2Sr_2CaCu_2O_x$ (Bi-2212), Bi_2SrCuO_x (Bi-2201), and $Bi_2Sr_2Ca_2Cu_3O_x$ (Bi-2223) ceramic compounds composed of strontium, bismuth, calcium, copper, and oxygen (27).

3.1.6 An Overview of superconductors Applications

In 1962, a group of researchers at Westinghouse produced the first wire of superconductors from titanium and niobium compounds, which was considered the first commercial superconducting wire at that time. Brian D. Josephson discovered that a current can flow between two superconductors separated by a thin insulating barrier. This phenomenon is known as the Josephson effect, and it is used to create sensitive magnetic sensors called superconducting quantum interference devices (SQUIDs). SQUIDs are used to measure very weak magnetic fields in a variety of applications, such as medical imaging, geophysics, and materials science (40). SQUIDs are essential components of highly sensitive magnetometers, voltmeters, amplifiers, and detectors. They are even used to measure brain activity in magnetically shielded rooms. SQUIDs can also detect magnetic waves, such as those from collapsing stars, and can be used in geological studies. However, the complex cooling system required for low-temperature SQUIDs has limited their widespread use. Another group of researchers found on HTS a synthesis of Tl, Ca, Ba, Cu, and Oxygen at the critical temperature of T=120K was reached. In 1993, the superconducting alloy of ($HgBa_2Ca_2Cu_3O_8$) and adding Hg instead of thallium, and the transition temperature was found to be T=133K (41). Many superconducting phase compositions of $Hg_{0.8}Tl_{0.2}Ba_2Ca_2Cu_3O_{8+x}$, which was obtained partially instead of thallium for mercury, the transition temperature T_c was raised up to 138K (42). Scientists are still trying to discover superconductive materials that are superconducting at room temperature.

3.2 (MgB_2) Magnesium Diboride

Magnesium diboride (MgB_2) was actually first synthesized by F. J. Morin, H. P. Bovenkerk, and J. T. Norton in 1953 at Bell Labs. Its superconducting properties were discovered in 2001 by Prof. J. Akimitsu and his colleagues. It was an amazing discovery because it consists of only two elements (magnesium and boron). Its components are so simple and abundantly available that it makes its production cheaper and easier. MgB_2, which is considered a metallic superconducting compound, has a high transition temperature of T_c=39K with good superconducting characteristics. Researchers discovered that magnesium diboride (MgB_2) is a promising superconducting material with several advantages over other superconductors, including a high transition temperature of 39K, impressive critical current density (J_c), affordability, increased flexibility, and capability. MgB_2 can be cooled using a cryogenic cooling system with much less power consumption due to higher working temperature instead of 4.2K, eliminating the need for expensive liquid helium cooling. This makes MgB_2 a suitable choice for digital cryo-electric technology that employs less costly cooling agents such as liquid neon (~15 K) or liquid hydrogen (43).

3.2.1 Magnesium Diboride: A Brief History

In 2001, a team of Japanies researchers led by Jun Akimitsu discovered superconductivity in magnesium diboride (MgB_2). Its transition temperature is lower than HTS materials, it exhibits a higher critical temperature compared to conventional supercondcutors like Nb_3Ge, Nb_3Sn, and NbTi.

In the same year, a research paper was published by Osborn et al. (44) on superconducting MgB_2 material. Osborn's study specifically focused on the density of states of phonons in an isotopically enriched polycrystalline samples of MgB_2

compound. The study analyzed the lattice vibration energies in relation to superconductivity and determined a phonon mechanism with moderately strong electron-phonon coupling (45).

3.2.2 MgB_2 Structure

Magnesium diboride (MgB_2) has a simple hexagonal structure, making it an attractive superconducting material. The basic structure of magnesium diboride MgB_2 is a simple hexagonal unit cell structure in a formula of AlB_2 by P6/mmm space group (46). The crystal structure of MgB_2 consists of layers of magnesium atoms arranged in a triangular lattice, with boron atoms located between these layers, forming a hexagonal lattice. The presence of the boron atoms plays a crucial role in the superconducting behavior of MgB_2 (47).

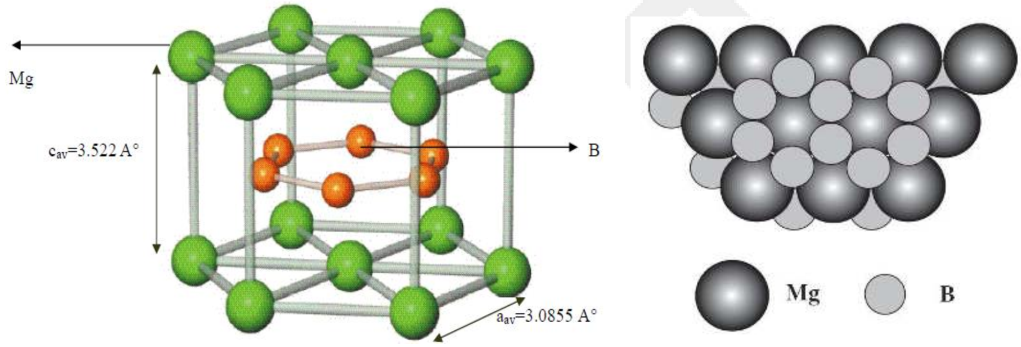

Figure 3.9. The structure of MgB_2 containing graphite-type B layers separated by hexagonal close-packed layers of Mg.

3.2.3 Properties of MgB_2

The crystal structure of MgB_2 is hexagonal, with lattice parameters a = 3.086 Å in the plane and c = 3.524 Å out of the plane. These parameters can vary based on the original atomic arrangement of magnesium and boron. The high transition temperature of magnesium boride (T=39K) arises from the strong interaction between lattice vibrations (phonons) and electrons. This interaction is a result of the specific structure of MgB_2 and the electron conductivity characteristics. Conductivity in MgB_2 is primarily determined by the electrons in the boron (B) layer. The conduction responsibility relies on the occupancy of electrons within this layer. In contrast, conductivity between the planes is significantly weaker. The transmission of electrons through interplane bonds is strongly influenced by vibrations in the interplane lattice. This interaction mechanism is governed by phonons, as per the principles of the BCS theory. This strong interaction, along with the formation of Cooper's pairs, enables the preservation of superconducting properties at elevated temperatures (48).

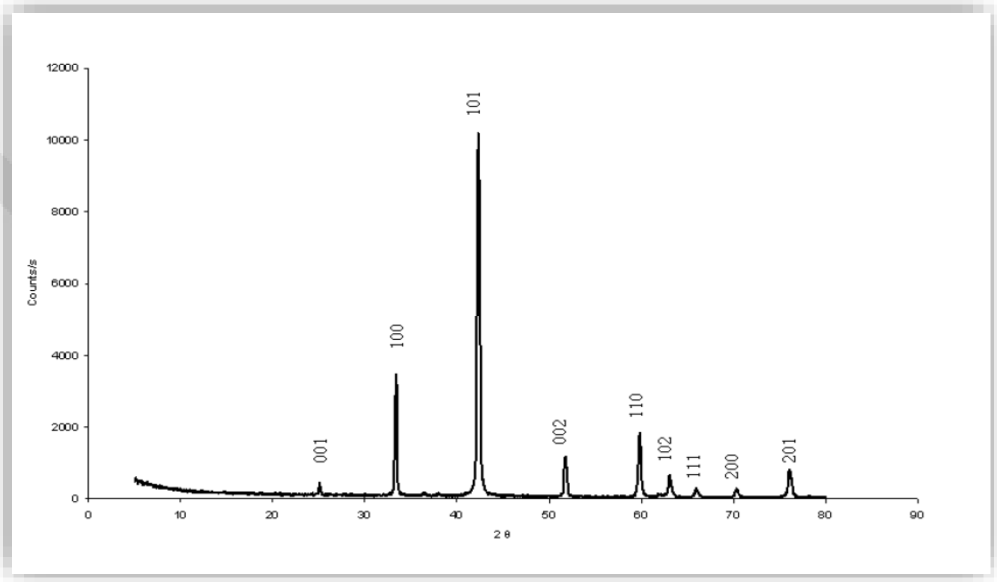

Figure 3.10. Representing of XRD pattern of commercial MgB_2 powder (49).

3.2.4 Applications of MgB2

Since 2001, Magnesium diboride (MgB_2) has attracted substantial attention from the scientific and research community owing to its distinct superconducting characteristics. It is now considered one of the most commonly used superconducting materials today. Magnesium diboride (MgB_2) is a highly promising material that holds great potential for various applications in advanced industries and technologies. Moreover, its production cost is relatively low due to the affordability of the raw materials involved. Thus, MgB_2 properties can be played a role in improving its applications a wide. One of the applications of MgB_2 is in high-power transformers, where it produces superconducting wires that can carry electric current at zero voltage which is considered the most important equipment in the magnetic coil which is used in medical and scientific instrumentation, namely magnetic resonance imaging (MRI) and also in particles acceleration. Unlike other borides, magnesium boride exists in a hydrolyzed form, allowing for the production of boron hydride compounds. Currently, superconductive materials technology diffusion is widely dependent on low-cost superconductors such as (Nb) based inter-metallic compounds. While these materials have lower critical temperatures than some other superconductors, they are easier and more cost-effective to produce for commercial purposes.

Scientists are actively working to further enhance MgB_2 superconductors, aiming to make MgB_2 an efficient replacement for conventional superconductors for various applications utilises superconducting wires and films (50).

4. FABRICATION TECHNIQUES OF MGB2 WIRES AND TAPES

The production of MgB_2 wires and tapes begins by filling metal tubes with MgB_2 powder. Since MgB_2 reacts with many common elements, such as aluminium and copper, it is important to choose a suitable tube material. Metals such as iron, steel, niobium, and nickel are chemically stable and can be used as sheathing materials, even though they have poor thermal and electrical conductivity (51). The diameter of the powder-filled metal tube is then reduced to a suitable value using processes such as swaging, drawing, or rolling. These procedures are straightforward for some superconducting materials that do not require sheathing, but they are challenging for ceramic MgB_2 due to its intermetallic structure (52).

MgB_2 wires and tapes are typically manufactured using either the continuous tube filling and forming (CTFF) method or the powder-in-tube (PIT) method, each offering its own set of advantages and disadvantages(48,53).

4.1 Powder-in-Tube (PIT) Technique

The Powder-in-Tube (PIT) technique is commonly used to create superconductive materials, and it offers two options for the fabrication process: In-situ PIT or Ex-situ PIT. This method is valued for its affordability and convenience, especially when working with easily deformable materials. However, it's worth noting that fabricating MgB_2 superconductors requires special attention and expertise. The ceramic MgB_2 powder inside the sheath is mechanically hard and brittle, so it needs support from a ductile sheathing material. When the composite is drawn, it tends to clump together instead of flowing through the tube/wire smoothly (54).

In a PIT process, the initial step typically involves preparing a clean, empty metallic tube. It is then filled with the appropriate powder mixture, followed by closure of the ends with materials like Al, Pb, etc. One end of the empty metal tube is closed while the other end remains open to allow for filling of the powder into the tube. The open end of the tube is similarly closed after filling. Subsequently, the packed metallic tube is prepared for the next step, which involves gradual size reduction through processes like drawing or groove rolling. When a long wire is obtained after mechanical deformation processes, it may be subjected to flat rolling to produce tapes, if the final intended product is a tape. For MgB_2 superconducting wires, a final sintering heat treatment is applied at a temperature between 650-1000°C, depending on the other fabrication parameters. Fabrication can be designed to produce monocore or multi-filamentary wires or tapes. To produce multifilamentary wires and tapes, the individual monocore superconducting wires are first grouped together into small cylindrical bundles. These bundles are then placed inside a metal tube and subjected to swaging, rolling, and drawing processes, which effectively elongate the composite and produce long wires. This process can be repeated multiple times to increase the number of filaments within the cross-section (55).

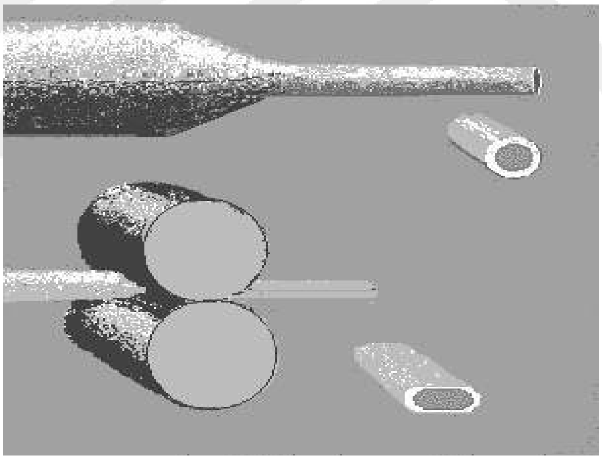

Figure 4.1. A simple fabrication of powder in tube (PIT) method.

MgB_2 exhibits high chemical reactivity, making it crucial to select an appropriate cladding metal to prevent defects such as electrical or chemical interactions from occurring. The sintering process needs careful adjustment since many metals have low melting points, which can chemically interfere with the sintering temperatures of MgB_2. This is due to the tendency of magnesium in MgB_2 to react with various metals, resulting in the formation of solid solutions or intermetallic compounds that further lower the melting point. Inert refractory metals such as niobium (Nb), tungsten (W), hafnium (Hf), vanadium (V), and molybdenum (Mo) are sufficiently hard and malleable to withstand the sintering process. However, materials like iron (Fe), stainless steel, and titanium (Ti) are more commonly chosen for cladding due to their ductility (56). It is important to note that the hardness of the ceramic MgB_2 core is not directly related to the sheath material's hardness, but the sheath material can indirectly impact the core's hardness by influencing the deformation process and the formation of intermetallic compounds. For instance, a harder sheath material might be harder to deform, resulting in a harder core. Moreover, the formation of intermetallic compounds between the core and sheath materials can affect the core's hardness while potentially disrupting the chemical stoichiometry (55,57).

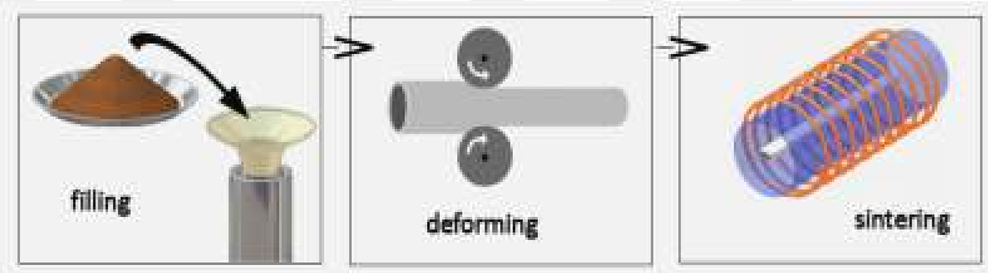

Figure 4.2. A simple fabrication of powder in tube method.

4.1.1 In-situ PIT Technique

Filling metallic tubes with a mixture of Magnesium (Mg) and Boron (B) powders, followed by a heat treatment process that induces deformation, is a crucial step in the In-situ PIT technique. Moreover, to achieve a high critical current density (J_c), it is essential to carefully select appropriate sheath materials and optimize the heat treatment process.

MgO forms in the MgB_2 core through the oxidation of magnesium, with impurity levels typically below 1% in high-purity magnesium and boron powders. While MgO can be present in both in-situ and ex-situ techniques, it is not necessarily formed in significant quantities. In the case of in-situ PIT processing, boron-rich phases often appear due to incomplete reaction of the precursor. However, there are several advantages to using the in-situ PIT technique, including lower reaction temperatures, less laborious mechanical fabrication, and a simplified doping process for MgB_2 phase. The occurrence of unwanted reactions with the powder is minimised due to reduced heat treatment temperature. Lastly, the closed-filled tube and packed powder must be chemically suitable for the reaction temperature of magnesium diboride (MgB_2) (58).

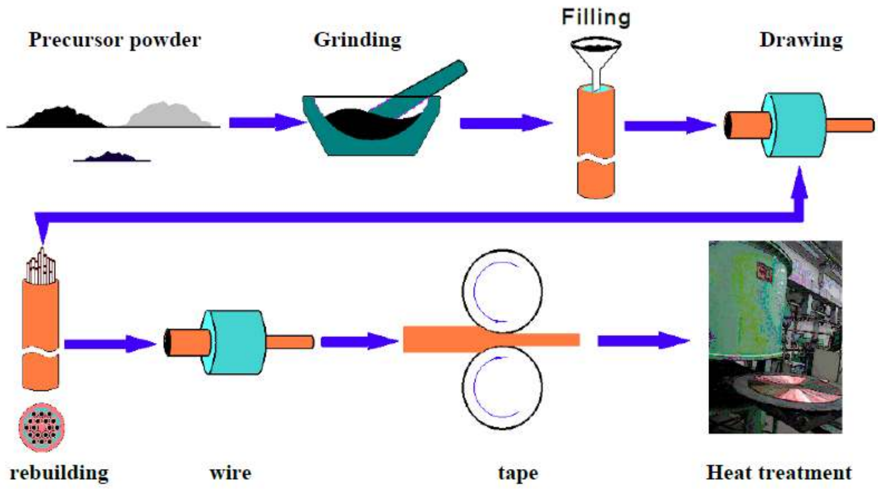

Figure 4.3. The in-situ PIT process for the fabrication of multi-filamentary MgB_2/Nb/Cu wires and tapes.

4.1.2 Ex-situ PIT Technique

Another technique is directly filling reacted MgB_2 powders into metallic tubes and followed by cold deformation. This fabrication is known as the ex-situ PIT technique. A suitable temperature in the heat treatment process may be kept higher compared to the in-situ process and it is between 600-1000°C to obtain an improved core density for superconductivity with well connected grains. Therefore, the sheath material choices are very limited when applying the high annealing temperature due to chemical reactions between the sheath materials and the filament's core, and this effect escalated in multi-filamentary wires with smaller core diameters. The thickness of the reaction layer typically ranges from 1 to 25 μm, depending on the heat treatment process and the sheath materials (59).

4.2 Continuous Tube Forming and Filling (CTFF) Technique

The Continuous Tube Filling-Forming (CTFF) process is a technique designed to enhance filling density. It involves pouring powders onto strips of metal during a continuous process. The filled tube is enclosed within another metal tube, typically Monel, to provide stabilization. Figure 4.4 provides a simplified schematic representation of the CTFF process. Initially, a wire with a metallic strip made of Niobium (Nb) is shaped into a symmetrical cylindrical tube after being filled with powder through a continuous process. Subsequently, the entire Nb tube, now containing the powder, is inserted into another metal tube, often made of a material like Monel. This double-sheathed tube is then prepared for drawing and rolling processes. All other superconducting wire production and fabrication methods use a batch process, in which metallic tubes of a fixed length are filled with powders and then mechanically deformed into wire. CTFF method does not require larger tubes to obtain longer lengths of superconducting wires. This method includes more wire fabrication processing, such as drawing, pressing, and extrusion, which is almost incurring high manufacturing and fabrication costs (60).

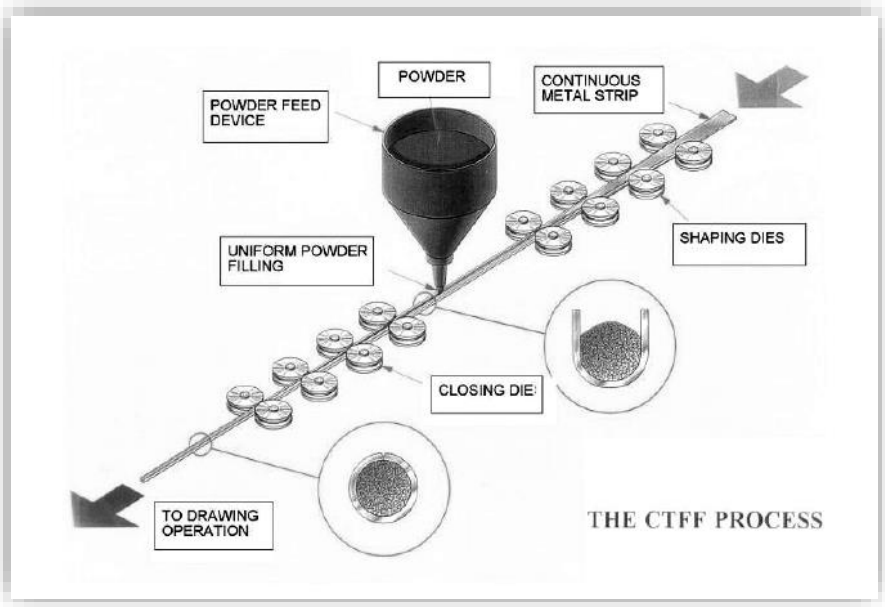

Figure 4.4. Sketch map of Continuous Tube Filling and Forming (CTFF) process.

4.3 Internal Magnesium Diffusion (IMD) Technique

Internal Magnesium Diffusion (IMD) is an effective technique to improve the packing factors that influence the critical current density J_c values of MgB_2 and in order to avoid the drawbacks of the PIT process. IMD technique exhibits and enhances much higher J_c value than PIT, either ex-situ PIT or in-situ PIT techniques. A high J_c was successfully achieved in the fabrication of MgB_2/Fe wires by Hur et al. (11) and Giunchi et al. (61). They applied the IMD technique as in Figure 4.5 by addition of SiC and using a pure magnesium rod. They placed a pure Mg rod with a diameter of (2 mm) centred in the iron tube. Then, boron B powders or a mixed powder of boron containing 5mol% of SiC was filled in the gap between the Mg and Fe tube. The composite was cold worked into a 1.2 mm wire diameter, and the heat treatment was performed above the melting point of magnesium, which is estimated to be 650°C. MgB_2 was formed throughout the heat treatment process, and the atoms of the solid magnesium rod react with boron when the latter infiltrated the B layers.

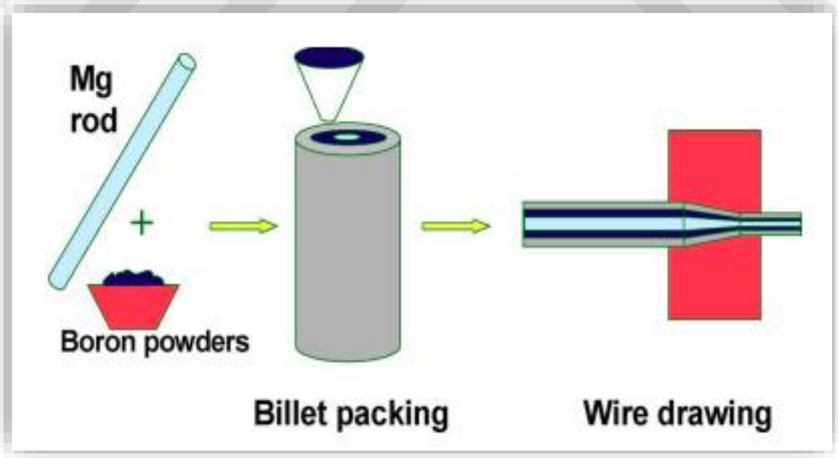

Figure 4.5. Steps of IMD process.

4.4 Sheath Materials

Magnesium diboride (MgB_2) is mechanically hard and forms brittle inter-metallic compounds like BSCCO and Nb_3Sn, which are more difficult to deform.

Therefore, the PIT process with a suitable sheath material is used for this brittle superconductor fabrication (62). The typical parameters of MgB_2 and other practical superconductors are shown in Table 4-1 (63).

Parameter	***NbTi***	***Nb_3Sn***	***MgB_2***	***YBCO***	***Bi-2223***
T_c (K)	9	18	39	92	110
Anisotropy	Negligible	Negligible	1.5~5	5~7	5~200
J_c at 4.2K (A/cm^2)	~10^6	~10^6	~10^6	~10^6	~10^7
H_{c2} at 4.2K (T)	11-12	25-29	15-20	>100	>100
H_{irr} at 4.2K (T)	10~11	21~24	6~12	5~7 (77K)	0.2 (77K)
Coherence length ζ (0) (nm)	4~5	3	4~5	1.5	1.5
Penetration depth λ (0) (nm)	240	65	100~140	150	150
Resistivity ρ (T_c) ($\mu\Omega$.cm)	60	5	0.4	150~800	40~60

Table 4.1. Fundamental superconducting properties of the practical superconductors.

The superconductor wire produced using the PIT method, along with a suitable sheath, is widely used for various applications. However, in terms of flexibility, it falls short when compared to conventional metallic wires. This limitation is primarily attributed to the choice of sheath materials. Typically, materials with high thermal and electrical conductivities like silver (Ag) and copper (Cu) are utilized for fabricating BSCCO superconductors. Unfortunately, these materials react strongly with magnesium and boron, resulting in the formation of a reaction layer that diminishes the wire's overall performance. To address this issue, MgB_2 wires and tapes are usually fabricated with a sheath made of stainless steel, iron, or niobium to avoid such reactions (51,62,64–66).

A crucial point is to reduce the reaction layer between the sheath material and the superconducting core, which can be done by using suitable sheath materials. There are many requirements for choosing a proper sheath material:

- It should be in chemical stability.
- Plasticity.
- Higher thermal and electrical conductivities.
- Lower cost.

Therefore, many materials are used as sheath materials in MgB_2 wire and tape fabrication by different groups, such as Stainless Steel (SS) (67), Cu (68–70), Fe (71,72), Ni (73), Nb (74), Ta (75,76), etc. Using an appropriate sheath material can enhance the mechanical strength of MgB_2 wires and tapes. Common sheath materials for MgB_2 include copper (Cu), niobium (Nb), and iron (Fe) owing to their affordability and favourable mechanical properties. When it comes to chemical compatibility with MgB_2, only niobium and iron are suitable options. Iron is particularly appealing due to its low cost, while niobium has the advantage of not reacting with magnesium and boron, but it is expensive. Despite its tendency to react with magnesium, copper offers good thermal stability and is relatively inexpensive. Furthermore, it is possible to utilize composite sheaths using different metal tubes, such as Fe-Cu, Fe-Ni, Cu-Ta, Cu-Ni, Fe-SS, etc., for both inner and outer cladding layers (48,51,62,64–66).

4.5 Annealing Temperature

There are two types of reactions due to the difference in melting points of Mg and B. The solid-solid reaction dominates at temperatures below 650°C, while the liquid-solid reaction dominates at temperatures above 650°C (77,78). The annealing temperature affects the crystal structure significantly. The crystal shape of the hexagonal structure is affected by heating slowly, while the fast heating process is favorable for the formation of needle crystals and thin plate crystals with rectangular shapes (79).

In 2005, Yamamoto et al. explained the influence of the reaction of solid-solid between magnesium and boron in bulk samples, while Serquis and his group found the effect of annealing temperature conditions on micro-structural improvement for higher critical current density J_c (80). Thus, The conclusion was obtained that high annealing temperatures are effective for enhancing the critical current density J_c because they lead to poor crystallinity, which in turn enhances the upper critical field and irreversibility magnetic field. This results in excellent pinning properties in high fields (81).

The influence of annealing temperature and heating rates on the critical temperature T_c and critical current density J_c for both doped and pure MgB_2 superconducting wires was reported by Chen et al. (82). Meanwhile, Zhao et al. (83) discussed the effects of heating rates microstructure level and how superconducting properties act on performance of MgB_2, they reached to temperatures of 1073°C with rates of 0.6, 0.9, 1.8 and 4 hours of duration. They observed at low temperatures, a different morphology causes changes in high field due to the connectivity of grain with applying a fast heating process in the presence of vacancies in the sample. The heat treatment process is an important parameter in the synthesis of MgB_2 that is related directly to the morphology and size of the grain and to the rate level of magnesium oxide MgO, which affects the current-carrying properties of MgB_2 (84). The relationship between current density and sintering temperature has been successfully investigated, but the impact of heating rates on the properties of superconducting materials has not been fully clarified (83,85).

In the case of pure MgB_2, the critical current density J_c drops gradually if an applied magnetic field is increased because of the weak pinning force. Moreover, substitutions other elements for boron, like carbon via compounds such as SiC and MgB_2C_2. The unit cell of MgB_2C_2 is shown in Figure 4.6. Carbon substitution for boron in MgB_2 is widely practiced for the improvement of flux pinning at high magnetic fields. In the case of fabrication of MgB_2, it's important to improve the critical current density J_c achieving a higher upper magnetic field. Improvement of the critical current density at higher applied magnetic fields by doping is considered the most effective method. The substituted carbon atoms are located at the boron sites, and the upper critical field can be increased this way. The porosity decreases during the sintering process while the connectivity increases among particles. Thus, the microstructure is more homogeneous. Therefore, the T_c critical transition temperature increases, causing the critical current density to increase, and if the T_c critical transition temperature gradually increases, this enhances the annealing temperature increases. According to this, the pores gradually close too. The annealing temperature depends on the process in which the samples are prepared (86).

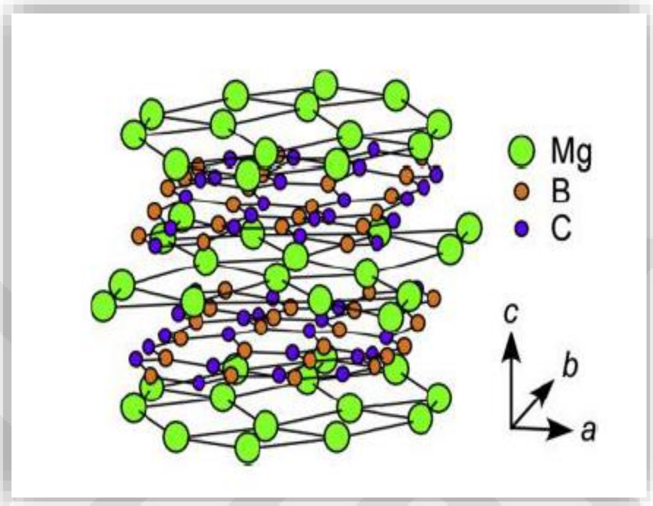

Figure 4.6. Crystal structure of MgB_2C_2 (87).

5. EXPERIMENTAL METHODS FOR MGB2 WIRES AND TAPES

5.1 Initial Powder Preparation in In-situ PIT Method

Mg+2B powder mixture was prepared from magnesium (99% purity, ~149-74 µm - particle sizes) and boron powders (Contains equal amounts of boron amorphous 95-97%, <1 µm - particle sizes) Purchased from PVZ Advanced Chemicals. Initially, the powders are weighed and mixed in a stoichiometric proportion based on the stoichiometry of MgB_2. Therefore, it is necessary to prevent magnesium oxide formation, the process was conducted inside a glove box under argon atmosphere, and the Mg+2B powder was mixed in the ball milling machine for three hours, as shown in Picture 5.1.

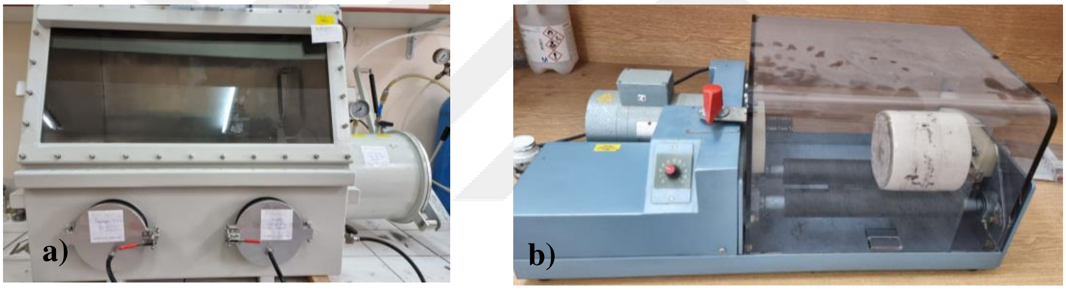

Picture 5.1. a) Glove box and b) Ball milling machine.

On the other hand, iron tubes used in the In-situ PIT method were selected to have an outer diameter of 15 mm and an inner diameter of 12 mm. Moreover, for 20 minutes, the iron tube was cleaned in acetone using an ultrasonic cleaner. After these steps, we closed one end of the tube with aluminium foil, filled the mixture of Mg+2B powder inside the tube, and closed the other with aluminium foil.

5.2 Production of MgB_2/Fe Monocore Wires and Tapes

In this step, MgB_2 superconducting wires and tapes were produced using the in-situ powder-in-tube (PIT) method, as described in the previous section. This involved first preparing a homogeneous mixture of Mg and 2B powders, and then packing it into an iron tube. The powder-in-tube method is suitable for the production of these wires and tapes. To begin with, the tube with a diameter of 15 mm underwent the groove rolling process using groove rolling machines. This process aimed to reduce its diameter to 3 mm. The groove rolling machines are shown in Figure 5.1. Following this step, the wires underwent cold drawing and were passed through multiple circular dies, as shown in Figure 5.2. The diameter of the wire sample at different stages of rolling and drawing steps are listed in Table 5.1, together with the length of the wire. Starting from 2.5 mm diameter, wire pieces were cut from the wire sample at diameters of 2.5mm, 2.0mm, 1.7mm and 1.3 mm were cut for later processing and measuring.

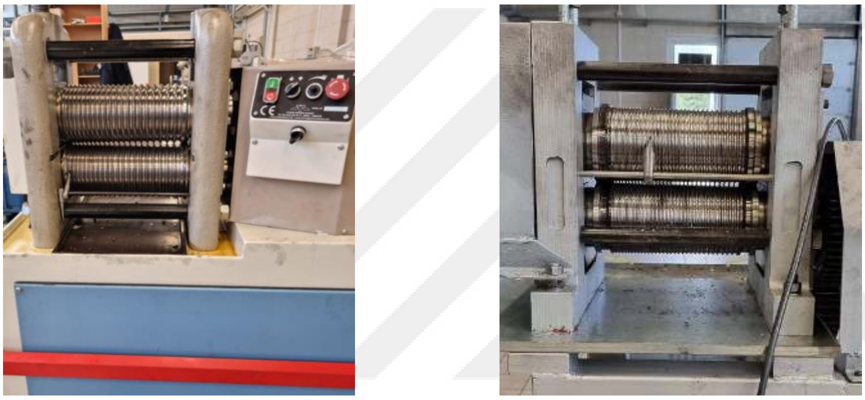

Figure 5.1. Groove rolling machines.

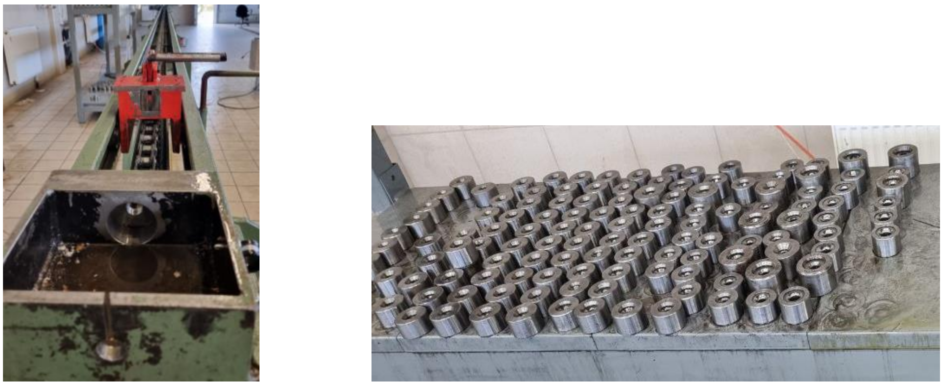

Figure 5.2. The machine for drawing long wires, and diameters of different dies.

Diameter of wire (mm)	Length of wire (cm)	Diameter of wire (mm)	Length of wire (cm)	Diameter of wire (mm)	Length of wire (cm)	Diameter of wire (mm)	Length of wire (cm)
15.00	125	**2.78**	670	**2.15**	693	**1.62**	322
8.10	280	**2.71**	708	**2.10**	712	**1.58**	348
7.30	335	**2.64**	748	**2.04**	751	**1.54**	359
6.30	479	**2.55**	803	**2.00**	776	**1.50**	372
5.50	600	**2.50**	831	**2.00**	446	**1.47**	406
4.00	1220	**2.50**	501	**1.95**	493	**1.43**	419
3.05	1350	**2.45**	527	**1.90**	500	**1.36**	444
3.03	555	**2.40**	543	**1.75**	594	**1.30**	518
2.99	583	**2.32**	603	**1.70**	620		
2.93	599	**2.27**	612	**1.70**	290		
2.85	644	**2.21**	637	**1.67**	301		

Table 5.1. Process of drawing MgB_2/Fe samples

Consequently, the flat rolling process of these wires was to produce tapes was carried out in the flat rolling device, as shown in Picture 5.2. During the flat rolling process, sections of the tape sample were cut at various thicknesses of 1.2 mm, 0.9 mm, 0.6 mm, and 0.4 mm. These cut sections were then heat-treated for further processing, followed by cryogenic measurements. In brief, the groove rolling, cold drawing and flat rolling process steps include intermediate heat treatments at a temperature below the synthesis temperature of MgB_2 to reduce the mechanical stress and remove the induced strain accumulated in the wires and tapes due to these operations.

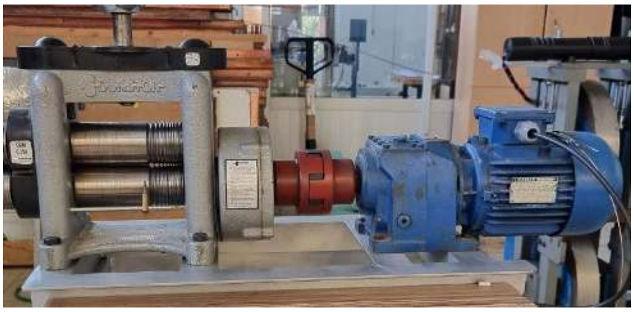

Picture 5.2. Flat rolling machine.

5.3 Process of Heat Treatments

Heat treatment is the last step in the MgB_2 synthesis process. After cutting samples of MgB_2 wires and tapes to specific lengths, the ends of the pieces were closed using a mechanical press, as shown in Picture 5.3 (a). The ends of the wires were closed to prevent the loss of magnesium from the ends during heat treatment. In addition, heat treatment was applied to all samples at 700 °C for 2 hours, using a tube furnace (protherm-model) under 5-10 bar pressure in a high-purity argon atmosphere, as shown in Picture 5.3 (b). After placing the MgB_2 samples in the furnace, the tube was evacuated to remove the air inside, then washed with argon gas, and evacuated again. Therefore, the process of discharging and adding argon gas is repeated three times under a pressure of 3 bar. After the washing with the argon gas process was completed, the tube was filled with argon gas at 5-10 bar pressure to prevent the oxidation of wire and tape samples. Finally, the furnace was set to the specified temperature for heat treatment.

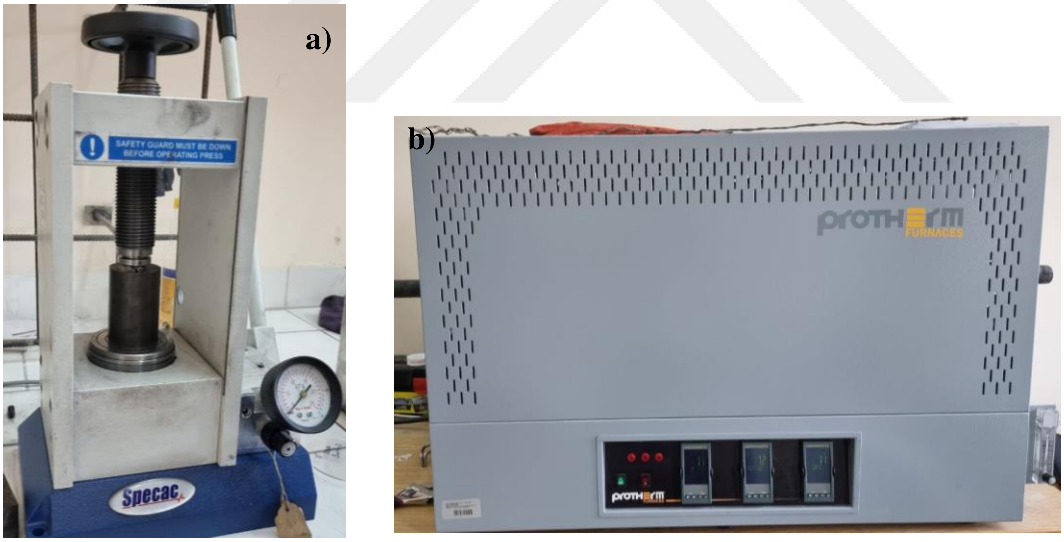

Picture 5.3. a) Mechanical press and b) Photograph of the furnace.

Picture 5.4. The samples after heat treatment.

5.4 Cryogenic Tests and Measurements

The superconducting transition resistivity-temperature (R-T) and current-voltage (I–V) measurements were made for all samples of MgB_2 wires and tapes using a helium cryostat system with a closed cycle. This measurement system can apply a magnetic field of (0 - 7 Tesla) and can drive a direct current (DC) in the range of 0-1 ampere. Initially, heat treated samples were cut to a length of (25 mm) then an ordinary Pb-Sn solder was used for the voltage and current contacts on these samples, as shown in Figure 5.3. Consequently, the samples were placed perpendicular to the magnetic field in the helium cryostat system. The samples to be measured were cooled in a zero magnetic field. On the other hand, the magnetoresistivity was measured, and a direct current of (50 mA) was applied between temperatures ranging from (4 - 50 K) to determine the critical temperature (T_c) of the samples. Moreover, the voltage (I–V) characteristics were measured at a constant temperature (25K) to determine the critical current density (J_c) and critical engineering current density (J_e) of the samples.

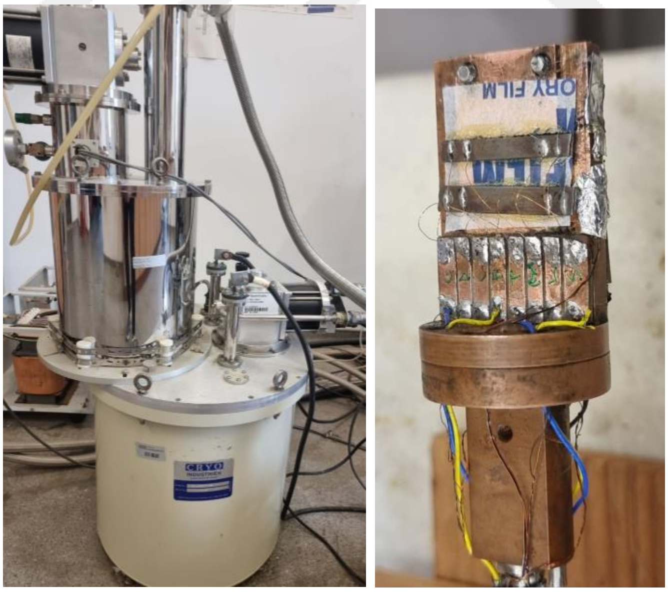

Figure 5.3. cryostat system for characterization of superconducting properties of samples.

5.5 Metallographic Studies

Initially, small samples of MgB_2 wires and tapes were placed vertically or longitudinally with copper acrylate powder using a mounting machine, as depicted in Picture 5.5 (a). Subsequently, molds containing the samples were obtained. Following that, polishing procedures were applied to these molds using SiC grinding papers of grades 240, 600, 1200, and 2500, as presented in Picture 5.5 (b). Lastly, the surface structures of the samples were examined using an optical microscope, as shown in Picture 5.6. The photographs taken from the optical microscope were then used to calculate the cross-sectional area of the samples.

Picture 5.5. a) Mounting machine and b) Polishing machine.

Picture 5.6. Optical microscope.

6. EXPERIMENTAL RESULTS AND DISCUSSION

6.1 Cross-sectional area change upon flat rolling

Swaging, groove rolling, cold drawing, and flat rolling processes are widely used to manufacture wires and tapes of various materials. In this part, we have investigated changes in cross-sectional area and elongation of monocore Fe/MgB_2 wires and tapes. The aim is to understand how material properties and dimensions affect deformation behavior during these processes. We performed the drawing and rolling process on wires and tapes of different diameters and thicknesses. We calculated the cross-sectional area and elongation, as shown in Table 6.1, where the samples were classified as follows: (W for wires) and (K, L, M, N for tapes), with subsequent letters indicating specific dimensions (A, B, C, D).

Moreover, the cross-sectional area decreases with decreasing wire diameter or tape thickness. This decrease in cross-sectional area is expected as the material is compressed in the rolling direction, reducing the cross-sectional area upon elongation. On the other hand, as the thickness decreased, elongation accelerated. Thicker wires elongated more, and thinner wires elongated less upon flat rolling.

In summary, the results show the changes in cross-sectional area and elongation during the drawing and rolling process of monocore Fe/MgB_2 wires and tapes. Therefore, the wires suffer less deformation than the tapes. Despite this, the tapes undergo stretching and deformation, which leads to a reduction in cross-sectional area and thickness and an increase in elongation. The rolling process can be controlled to improve the manufacturing process and material performance in practical applications.

Samples Code	Wire diameter (mm)	Tape thickness (mm)	Total cross-Sectional area (cm^2)	Core area (cm^2)	Voltage tips distance (cm)	Elongation (%)
WA	2.5	———	0.04835	0.02523	1.365	None
KA	———	1.2	0.03806	0.01974	1.565	12.9
LA	———	0.9	0.03611	0.01839	1.652	35.8
MA	———	0.6	0.02336	0.01122	1.615	63.5
NA	———	0.4	0.01716	0.00742	1.366	109.8
WB	2.0	———	0.03223	0.01606	1.698	None
KB	———	1.2	0.03159	0.01516	1.475	4.3
LB	———	0.9	0.02802	0.01363	1.507	19.7
MB	———	0.6	0.01912	0.00884	1.436	39.5
NB	———	0.4	0.01412	0.00697	1.375	85.1
WC	1.7	———	0.02259	0.01252	1.589	None
KC	———	1.2	0.02167	0.01014	1.488	1.5
LC	———	0.9	0.02282	0.01049	1.537	10.4
MC	———	0.6	0.01694	0.00756	1.544	26.1
NC	———	0.4	0.01313	0.00749	1.567	64.4
WD	1.3	———	0.01351	0.00729	1.446	None
LD	———	0.9	0.01407	0.00728	1.531	2
MD	———	0.6	0.01155	0.00585	1.559	9.8
ND	———	0.4	0.00989	0.0048	1.541	38.5

Table 6.1. Total cross-sectional area, core area, voltage tips distance, and elongation values for MgB_2/Fe monocore wires and tapes samples.

6.2 The Measurements of resistivity - temperature (ρ-T)

Resistivity versus temperature measurements of monocore Fe/MgB_2 wires and tapes were made in the range of 5K - 45K. These samples were heat treated at 700°C for 2 hours. In these tests, a direct current of 50 mA was applied. Furthermore, the tests conducted on MgB_2 wire and tape samples helped determine their critical temperature, denoted as T_c. The critical temperature value of a sample is closely associated with its superconductivity. Table 6.2 shows the critical temperature values $T_{c\ offset}$, $T_{c\ onset}$, temperature change ($\Delta T=T_{c\ onset}-T_{c\ offset}$), and normal state resistivity (NSR).

Samples Code	Wire diameter (mm)	Tape thickness (mm)	$T_{c\ offset}$ (K)	$T_{c\ onset}$ (K)	ΔT (K)	NSR (μΩ.cm)
WA	2.5	———	37.71	38.92	1.21	236
KA	———	1.2	37.39	38.80	1.41	122
LA	———	0.9	36.81	38.45	1.64	192
MA	———	0.6	36.72	38.04	1.32	68
NA	———	0.4	36.28	38.13	1.85	219
WB	2.0	———	37.38	38.45	1.07	233
KB	———	1.2	37.76	38.86	1.1	131
LB	———	0.9	37.03	38.59	1.56	222
MB	———	0.6	37.09	38.68	1.59	181
NB	———	0.4	36.81	38.39	1.58	231
WC	1.7	———	37.87	38.94	1.07	150
KC	———	1.2	37.25	38.48	1.23	105
LC	———	0.9	36.74	38.21	1.81	168
MC	———	0.6	37.32	38.87	1.55	165
NC	———	0.4	36.96	38.38	1.42	112
WD	1.3	———	37.73	38.79	1.06	227
LD	———	0.9	36.71	38.04	1.33	152
MD	———	0.6	36.95	38.36	1.41	160
ND	———	0.4	36.72	38.18	1.46	208

Table 6.2. $T_{c\ offset}$, $T_{c\ onset}$, ΔT, and NSR values for MgB_2/Fe monocore wires and tapes samples.

Figure 6.1 (a) shows the ρ-T curves. The WA sample shows the highest T_c at (37.71 K), while the NA sample shows the lowest T_c at (36.28 K). However, the range of temperature change at which superconductivity (ΔT) occurs varies between samples. Smaller tape thickness corresponds to a broader temperature range. The LA and NA samples have larger ΔT values than the others, indicating better stability over the temperature range.

On the other hand, the normal state resistivity values show a significant variation among the samples. The MA sample has the lowest resistivity (68 μΩ.cm), while the WA sample shows the highest resistivity at (236 μΩ.cm). In a nutshell, in comparison between the samples, the WA sample shows the best superconducting properties because it has the highest critical temperature.

Figure 6.1 (b) shows relatively close values of the critical temperature T_c for the samples. The sample KB has the highest critical temperature at (37.76 K), while the sample NB has the lowest critical temperature at (36.81 K). In addition, the values of temperature change ΔT for all samples range (from 1.07 K to 1.59 K). Where a decrease in ΔT indicates a sharper transition in superconductivity, on the other hand, the resistivity values are different for each sample. The WB sample contains the highest resistivity at (233 μΩ.cm), while the KB sample contains the lowest resistivity at (131 μΩ.cm). Otherwise, LB, MB, and NB samples have similar resistivity values. Finally, the results indicate that the KB tape sample that 1.2 thickness possesses the most suitable properties for superconducting than the other samples due to its higher T_c, lower resistivity, and sharper transmission.

Figure 6.1 (c) shows that the critical temperature T_c values for the samples fall within a range from 36.74K for the LC sample to 37.87K for the WC sample. Therefore, the WC sample is better than the other samples because it has the highest critical temperature T_c. In addition, the values of temperature change ΔT range from 1.07K to 1.81K, indicating that the superconducting transitions in all samples are relatively sharp. On the other hand, when comparing resistivity values, lower resistivity values indicate better conductivity. Sample KC has the lowest resistivity value of 105 μΩ.cm followed by sample NC at 112 μΩ.cm. Thus, the LC sample has the highest resistivity at 168 μΩ.cm among the samples.

Figure 6.1 (d) shows that the critical temperature T_c values for the samples fall within a range from 36.71K for the LD sample to 37.73K for the WD sample. However, the values of temperature change ΔT range from 1.06K to 1.46K. Additionally, the resistivity varies across the samples. Sample LD has the lowest resistivity value of 152 μΩ.cm followed by sample MD at 160 μΩ.cm. Thus, the WD sample has the highest resistivity at 227 μΩ.cm among the samples. Moreover, the WD sample is better than the other samples because it has the highest critical temperature T_c at 37.73K.

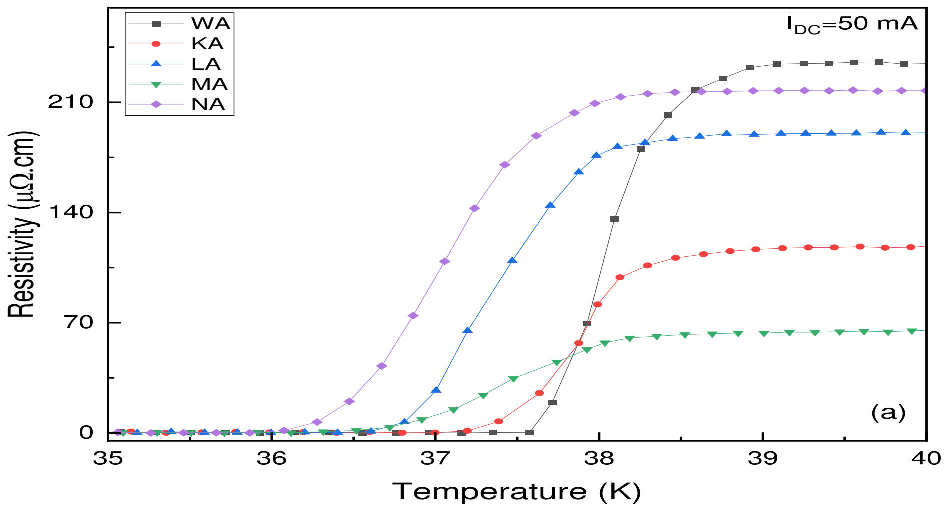
WA
KA
LA
MA
NA
I$_{DC}$=50 mA
Resistivity (μΩ.cm)
0
70
140
210
35
36
37
38
39
40
Temperature (K)
(a)

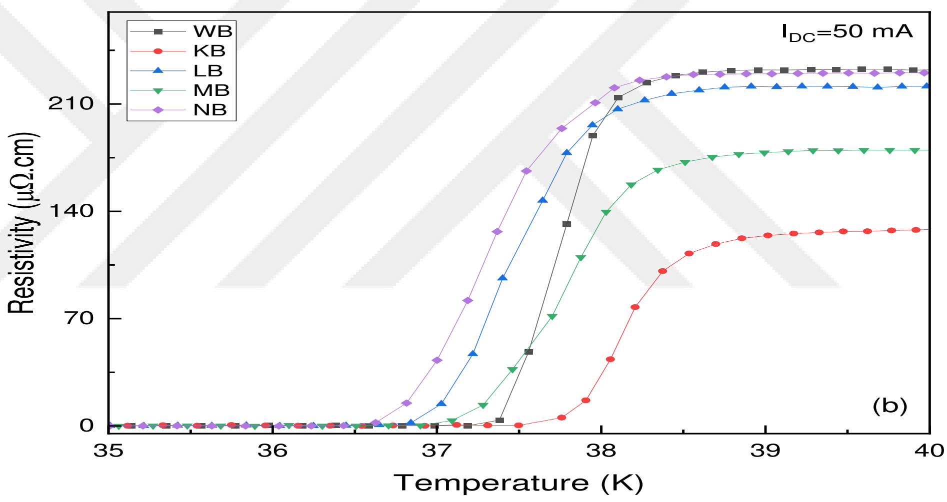
WB
KB
LB
MB
NB
I$_{DC}$=50 mA
Resistivity (μΩ.cm)
0
70
140
210
35
36
37
38
39
40
Temperature (K)
(b)

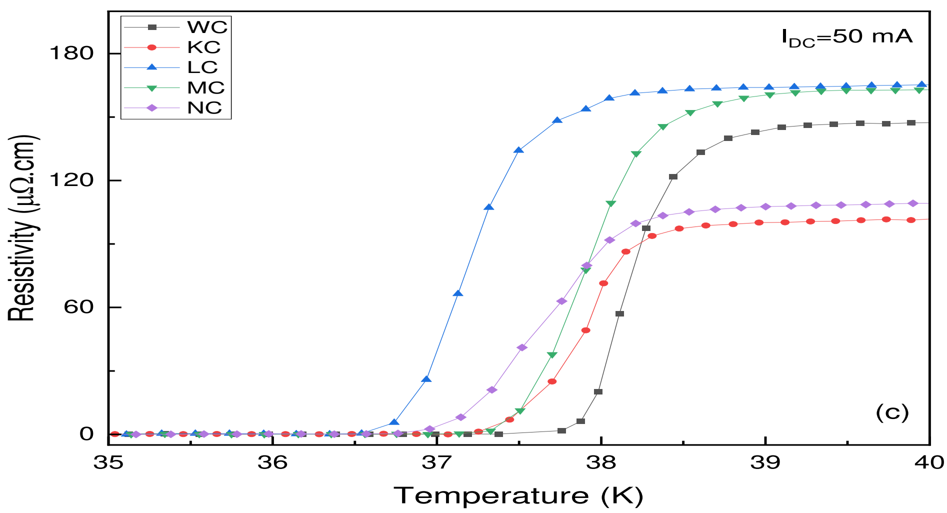
WC
KC
LC
MC
NC
I$_{DC}$=50 mA
Resistivity (μΩ.cm)
0
60
120
180
35
36
37
38
39
40
Temperature (K)
(c)

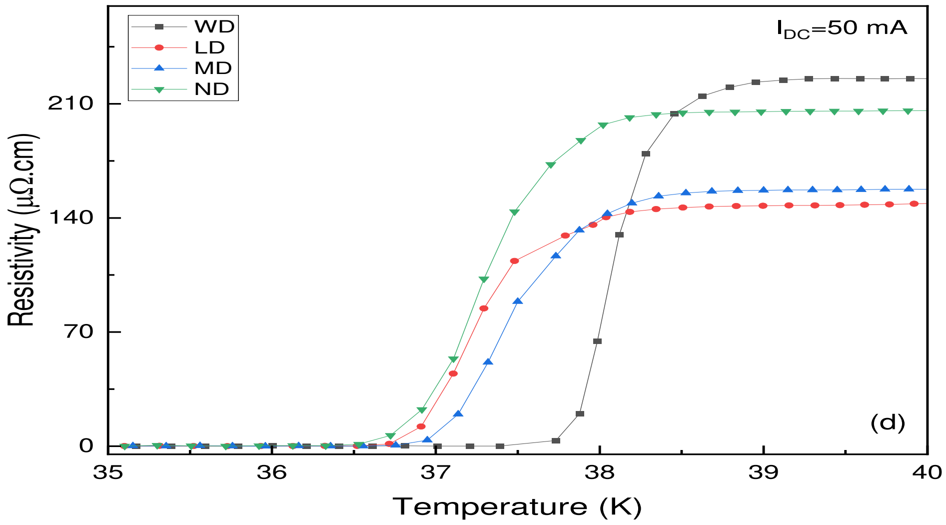

Figure 6.1.(a), (b), (c), (d) ρ vs. T curves for MgB_2/Fe monocore wire and tape samples. Samples were produced using the in-situ PIT method heat treated at 700°C for 2 hours. W means wire. K, L, M, and N mean tapes of thicknesses (1.2, 0.9, 0.6, 0.4 mm). A, B, C, and D mean wires of diameters (2.5, 2.0, 1.7, 1.3 mm).

6.3 The Measurements of current-voltage (I-V)

The current-voltage characteristics of the wires and tapes were measured at 25K with the standard four-probe method under a magnetic field ranging between 4T and 5.2T using the cryostat system. A maximum current of 1 ampere was applied to the samples to prevent excessive joule heating, and the perpendicular magnetic field was applied during measurements. On the other hand, all wire and tape samples have different cross-sectional areas and they exhibited transition at different magnetic field B values. However, when comparing the B values of all samples, it appears that the sample with the largest cross-sectional area has a higher magnetic field, and the samples with a lower cross-sectional area have a lower magnetic field. Consequently, the samples with larger cross-sectional areas maintain the superconducting state for a higher magnetic field before transitioning to the normal conductivity state. The table 6.3 shows J_e values and the magnetic field values at which they showed transition to normal state.

Samples Code	J_e (A/cm^2)	B (T)	Samples Code	J_e (A/cm^2)	B (T)
WA	13	5.2	**WC**	8	4.8
KA	10 13	5.2 5.0	**KC**	10 20	4.8 4.5
LA	4 13	5.0 4.5	**LC**	19	4.5
MA	10 21	4.5 4.0	**MC**	21	4.5
NA	9	4.0	**NC**	8	4.5
WB	21	4.8	**WD**	27	4.5
KB	12 7	4.8 5.0	**LD**	20	4.5
LB	5 21	5.0 4.5	**MD**	26 No.Tr	4.5 4.0
MB	9 31	4.5 4.0	**ND**	22	4.0
NB	18	4.0			

Table 6.3. Critical engineering current density (J_e) and magnetic field (B) values for MgB_2/Fe monocore wires and tapes samples.

Figures 2 through 10 show the E-J curves for all samples. Figure 6.2 depicts the E-J curves of the samples in group A. This group includes a wire sample with a diameter of 2.5 mm (WA), as well as tape samples that were flat rolled from a 2.5 mm diameter wire to achieve various thicknesses: 1.2 mm (KA), 0.9 mm (LA), 0.6 mm (MA), and 0.4 mm (NA). Firstly, when we compare the WA sample and the KA sample in a magnetic field of 5.2T, the WA sample demonstrates better performance, even though the difference in J_e (current density) is not significant. However, the resistivity at a current density of 55 A/cm^2 is almost twice that of the KA sample. Moving on, when comparing the KA sample and the LA sample at 5.0T, the KA sample outperforms the LA sample, and the difference between them is more noticeable. Similarly, when comparing the LA sample with the MA sample at 4.5T, the LA sample exhibits better performance, with the largest difference observed in resistivity values between them. Lastly, when comparing the MA sample and the NA sample at 4.0T, the MA sample surpasses the NA sample, and the differences in J_e and resistivity values are significantly larger.

We conducted this comparison because the cryogenic system we used can handle transport currents up to 1 ampere. However, not all the samples show a transition within the 0-1A current range. Therefore, in order to maintain the transition within this range, we needed to apply different external magnetic fields to the samples.

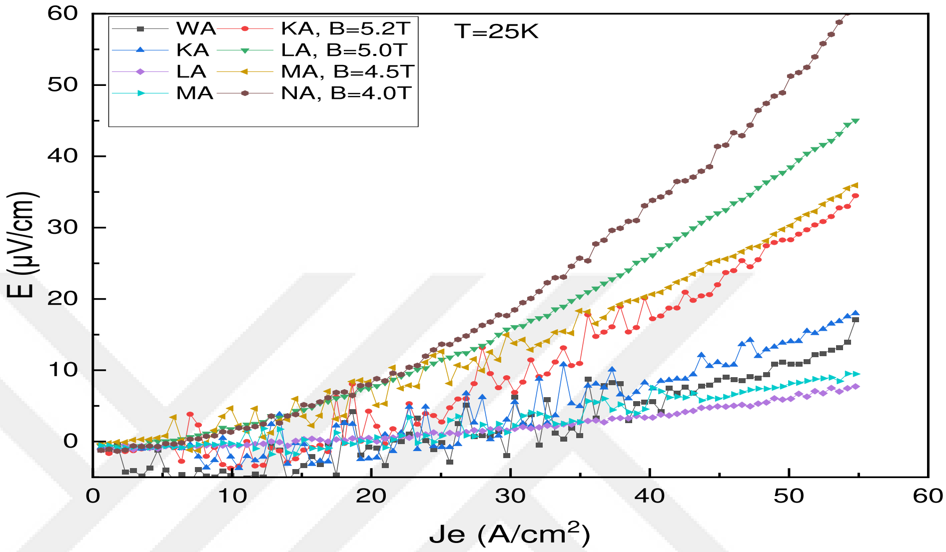

Figure 6.2. E vs. J_e curves for WA, KA, LA, MA, and NA samples under various external magnetic field values.

Figure 6.3 presents a comparison of the samples. Firstly, in a 4.8T magnetic field, the WB sample performs better than the KB sample. Secondly, when comparing the KB sample with the LB sample at 5.0T, the KB sample is better, although the difference is not significant. Thirdly, when comparing the LB sample with the MB sample at 4.5T, the LB sample demonstrates better performance, and the difference is more pronounced. Additionally, when comparing the MB sample with the NB sample at 4.0T, the MB sample outperforms the NB sample, and the difference between them is even more significant.

On the other hand, the curves for WB at 4.8T, LB at 4.5T, and MB at 4.0T appear very similar. However, the curves for KB at 5.0T, MB at 4.5T, and NB at 4.0T exhibit similarities.

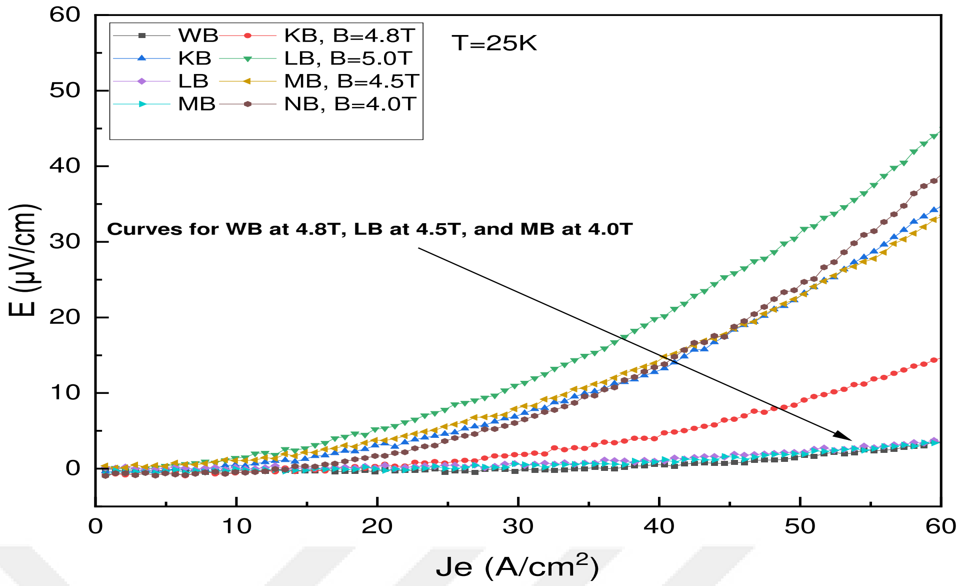

Figure 6.3. E vs. J_e curves for WB, KB, LB, MB, and NB samples under various external magnetic field values.

Figure 6.4 presents a comparison of the different samples within group C. Firstly, when comparing the KC sample to the WC sample under a magnetic field of 4.8T, the KC sample shows a slight advantage, although the difference is minimal. For all the other samples, there is a transition observed under the same magnetic field of 4.5T. KC, LC, and MC exhibit very similar E-J curves, with KC performing slightly better than the others, while MC demonstrates the highest resistivity. The engineering critical current densities of these three samples are closely matched. However, when considering the performance of NC at 4.5T, it is significantly worse than the other samples, with a much lower engineering critical current density.

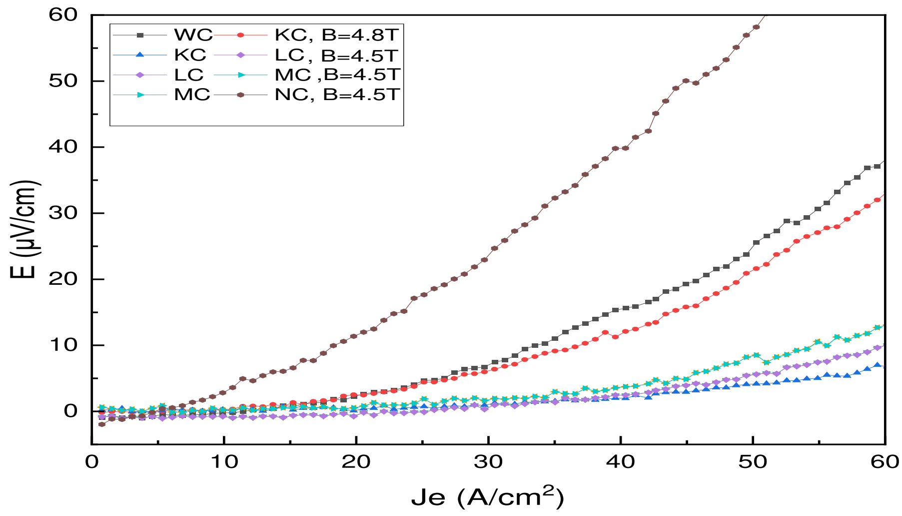

Figure 6.4. E vs. J_e curves for WC, KC, LC, MC, and NC samples under various external magnetic field values.

Figure 6.5 displays the E-J performances of the samples within group D. Initially, the WD, LD, and MD samples demonstrated a transition at a magnetic field of 4.5 T. The behaviors of WD and MD are quite similar, while LD exhibits a lower engineering critical current density and higher resistivity. When comparing the E-J curves of MD and ND obtained under 4T, ND exhibits the poorest behavior among these samples.

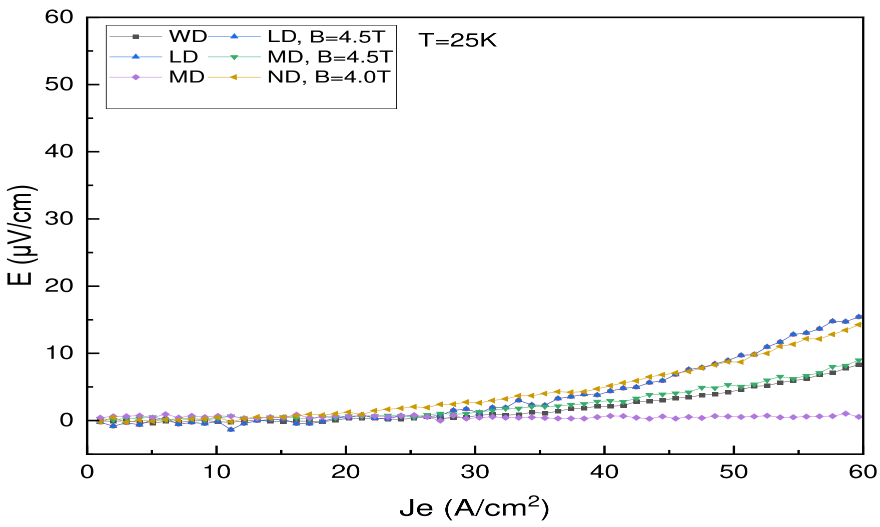

Figure 6.5. E vs. J_e curves for WD, LD, MD, and ND samples under various external magnetic field values.

Figure 6.6 shows comparison wire samples with diameters of 2.5mm, 2mm, 1.7mm, and 1.3mm. The WA sample outperforms the WB sample in a 5.1T magnetic field, with a significant difference in resistivity and engineering critical current density. At 4.9T, the WB sample outperforms the WC sample, with an even larger difference in resistivity and engineering critical current density. At 4.6T, the WC sample exhibits the poorest performance. In this analysis, it is more important to highlight the significance of a transition at higher magnetic field values than to focus solely on the higher engineering critical current density, as the range of current density values is narrow due to experimental limitations.

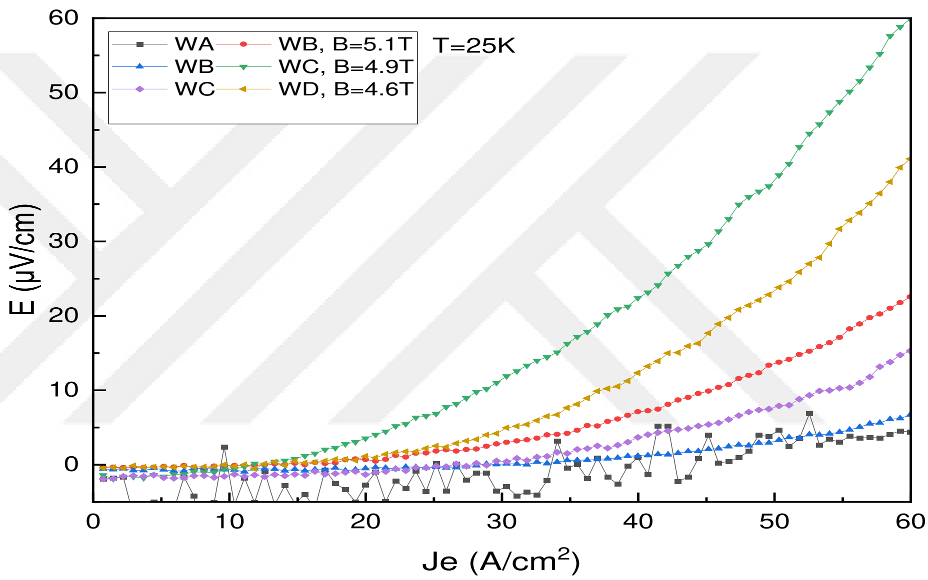

Figure 6.6. E vs. J_e curves for WA, WB, WC, and WD samples under various external magnetic field values.

Figure 6.7 presents a comparison between the tape samples KA, KB, and KC, all with a thickness of 1.2 mm. These tapes are flat rolled from wires with diameters of 2.5mm, 2mm, and 1.7 mm, respectively. The descending list in terms of performance is KA, KB, and KC. When comparing the E-J curves of KA and KB at 5T, KA demonstrates better performance in terms of engineering critical current density and resistivity. Similarly, comparing the E-J curves of KB and KC shows that KB outperforms KC in the same terms. We did not include sample KD since it would serve no purpose to create a tape of 1.2mm thickness from a wire with a 1.3mm diameter.

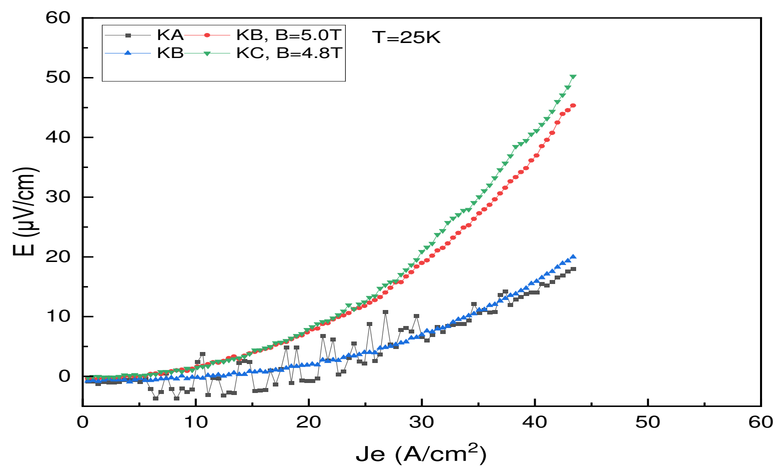

Figure 6.7. E vs. J_e curves for KA, KB, and KC samples under various external magnetic field values.

In Figure 6.8, we can see a comparison of tape samples LA, LB, LC, and LD, all with a thickness of 0.9 mm. These tapes are produced by rolling flat wires with respective diameters of 2.5mm, 2mm, 1.7mm, and 1.3mm. At 4.9T, the E-J curves of LA and LB reveal very similar behavior, with LA showing slightly lower resistivity, which is advantageous for superconductivity. When LB and LC were tested at 4.7T, it was observed that LC performed inferiorly compared to LB, and this difference was even more pronounced than the difference seen between LA and LB. In the final test conducted at 4.5T, LD exhibited a lower engineering critical current density and higher resistivity compared to LC.

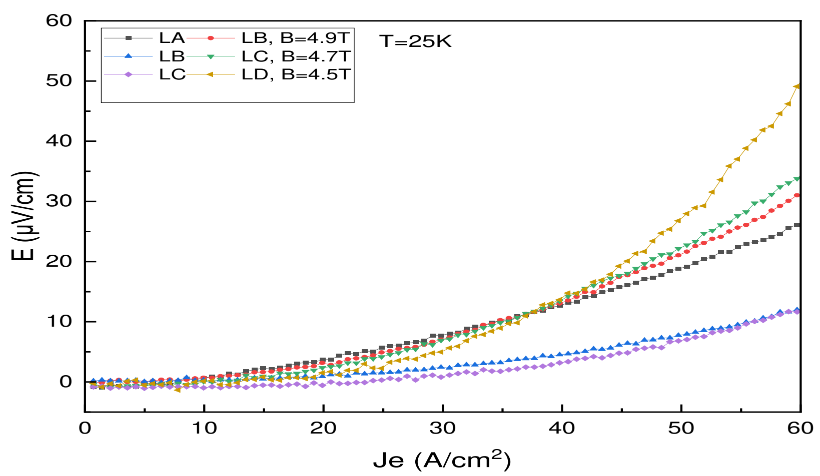

Figure 6.8. E vs. J_e curves for LA, LB, LC, and LD samples under various external magnetic field values.

Figure 6.9 presents a comparison of tape samples with a thickness of 0.6mm. The MA sample demonstrates a better performance compared to the MB sample in a magnetic field of 4.8T. Additionally, the MC sample shows the best performance when compared to the MB sample at 4.5T, exhibiting the largest difference. Similarly, the MC and MD samples exhibit similar performance at 4.5T, MD showing a higher resistivity. The MD sample achieved the highest engineering critical current density value of 26 A/cm^2 at a magnetic field of 4.5T.

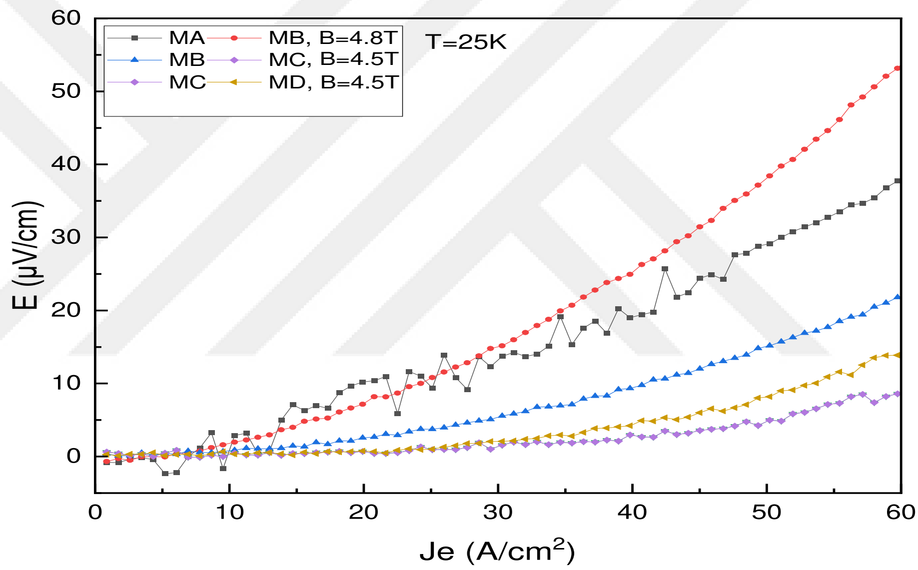

Figure 6.9. E vs. J_e curves for MA, MB, MC, and MD samples under various external magnetic field values.

Figure 6.10 presents a comparison of tape samples with a thickness of 0.4 mm, representing the thinnest samples. The NA, NB, NC, and ND samples are obtained by flat rolling wires measuring 2.5mm, 2mm, 1.7mm, and 1.3mm in diameter, respectively. On average, these samples exhibit lower performance compared to the thicker tapes. Examining the E-J curves in Figure 6.10, it can be observed that NB, NC, and ND samples behave similarly at 4T, with the ND sample achieving the highest J_e value of 22 A/cm^2 at this magnetic field. When comparing the performances of NA and NB at 4.2T, NA shows poorer performance, possibly due to excessive deformation resulting from the flat rolling starting with a 2.5mm wire.

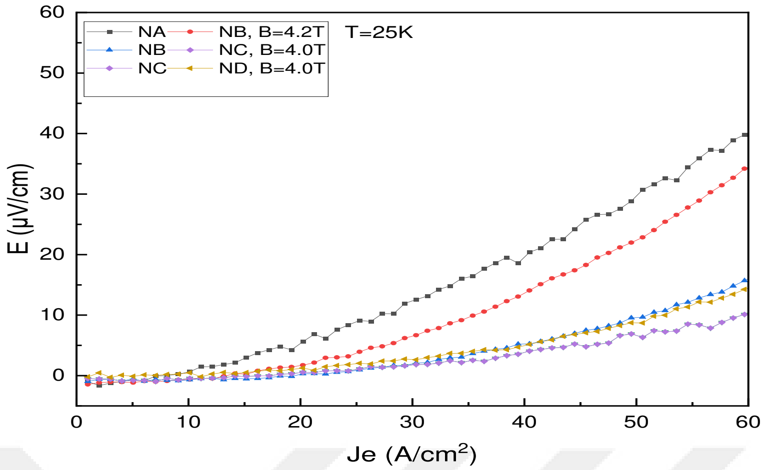

Figure 6.10. E vs. J_e curves for NA, NB, NC, and ND samples under various external magnetic field values.

The figures below show the critical engineering current density behaviors with the magnetic field J_e-B for all MgB_2/Fe monocore wire and tape samples made by the in situ-PIT method. When the magnetic field B of the samples increases, the critical engineering current density decreases because higher magnetic fields negatively affect transport properties of superconductors.

According to Figure 6.11 (a,b,c,d), samples with larger dimensions (wire diameter or tape thickness) tend to have higher J_e values. Tapes of smaller thickness show faster degradation of J_e, which makes them less suitable for applications involving strong magnetic fields.

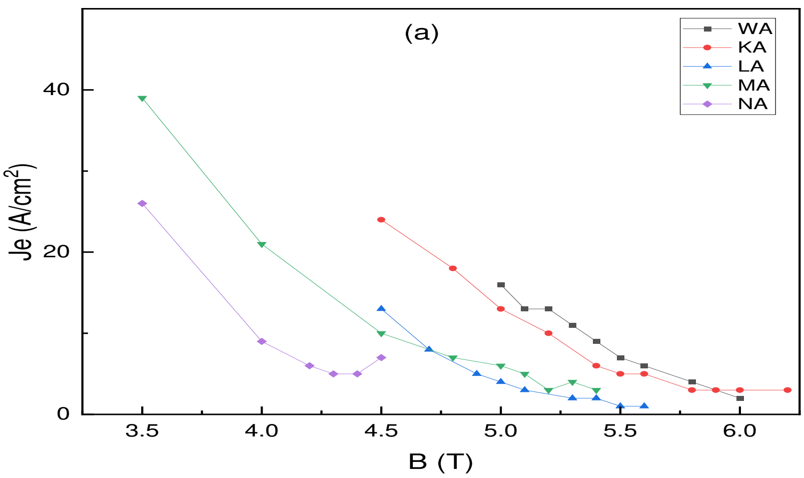

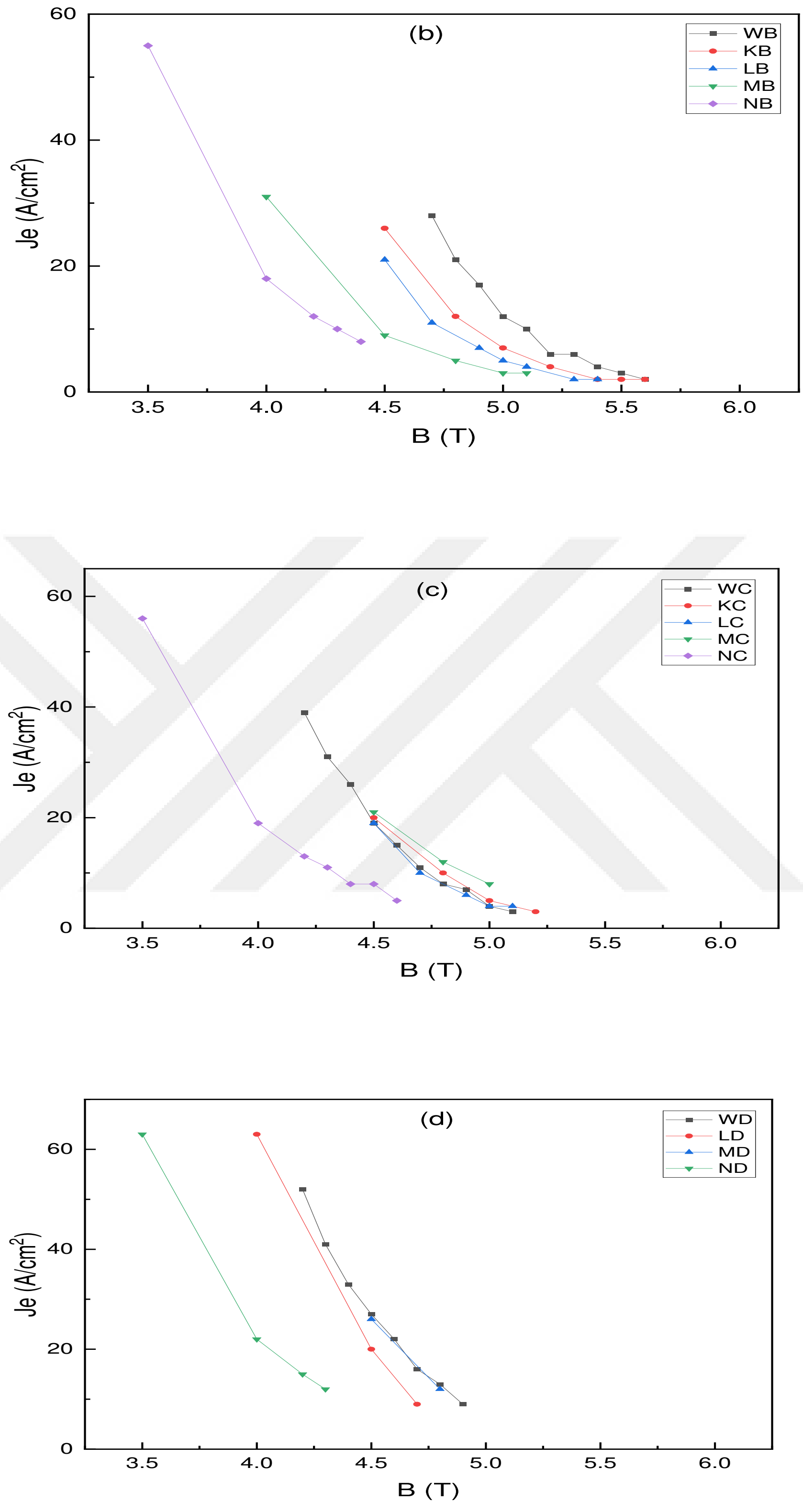

Figure 6.11. J_e vs. B curves for a) WA, KA, LA, MA, and NA samples, b) WB, KB, LB, MB, and NB samples, c) WC, KC, LC, MC, and NC samples, and d) WD, LD, MD, and ND samples.

Figure 6.12 shows the relationship between J_e and B for wire samples (WA, WB, WC, WD) with different diameters (2.5, 2.0, 1.7, 1.3 mm). The critical engineering current density represents the maximum current density the wire can carry before it loses its superconductivity. The wire's ability to carry current without resistance decreases as the magnetic field increases. Within the experimentally tested graphic area, performance of the wires deteriorate with decreasing wire diameter. Moreover, wire diameter plays an important role, as wires with smaller diameters (WC, WD) show a slower rate of decrease in J_e than wires with larger diameters (WA, WB).

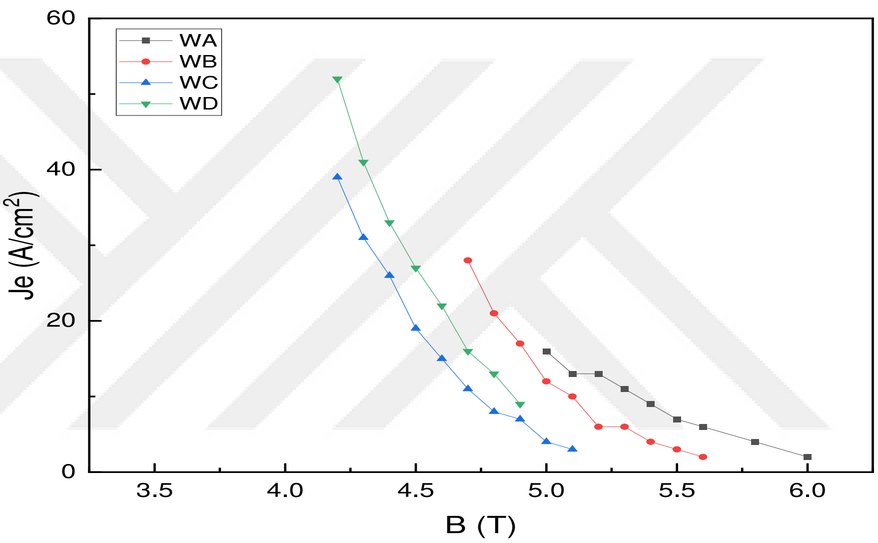

Figure 6.12. J_e vs. B curves for wire samples (WA, WB, WC, WD) of different diameters (2.5, 2.0, 1.7, 1.3 mm).

Figure 6.13 (a,b,c,d) shows sample tapes, all exhibiting typical behavior. The critical engineering current density J_e decreases with increased magnetic field strength B, which is not unexpected. Moreover, the samples with larger thicknesses show a higher critical engineering current density in the in lower current density-higher magnetic field region at 25K. In contrast, the samples with smaller thicknesses show lower critical engineering current density.

The engineering critical current density of the samples under applied magnetic fields depends on the tape thickness. This highlights the significance of tape thickness in determining the capacity of the samples to carry critical current. For 1.2mm thick tape samples, they carry higher supercurrents at higher magnetic fields when they are made from larger diameter wires. There appears to be some crossover behavior between samples KA and KB. At 5.5T, KA carries more supercurrent than KB, but at 4.5T, the opposite is true. This crossover behavior suggests that comparing samples in the low magnetic field - high transport current region may present a different scenario. For the tape samples coded starting with L, 0.9mm thick tapes, it seems that the effect of the diameter of the starting wire does not have a significant effect. However, the tape sample LA, produced starting from 2.5mm diameter wire exhibits the lowest engineering critical current density at 4.5T but it remains superconducting up to 5.6T. For tape samples coded with M and measuring 0.6mm in thickness, it has been observed that when these samples are fabricated using smaller diameter wires, they demonstrate higher critical engineering current densities at or below 4.5T applied magnetic field. Once again, we observe that the 0.6mm thick tape sample MA, which is produced starting with a 2.5mm wire, maintains its superconductivity up to around 5.5T applied magnetic field. The 0.4mm thick tape samples (NA, NB, NC and ND) appeorently demonstrate that transport current density performance is better when the tape is flat rolled starting from a smaller wire diameter, the MA sample being the worst one in this respect.

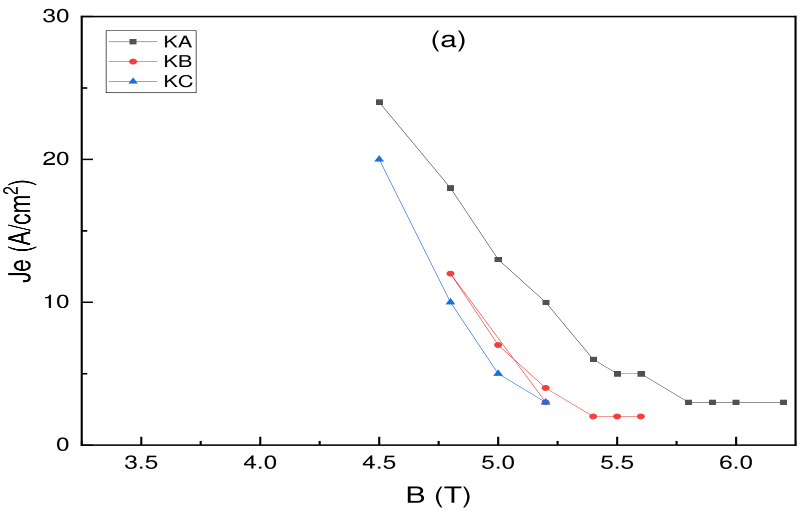

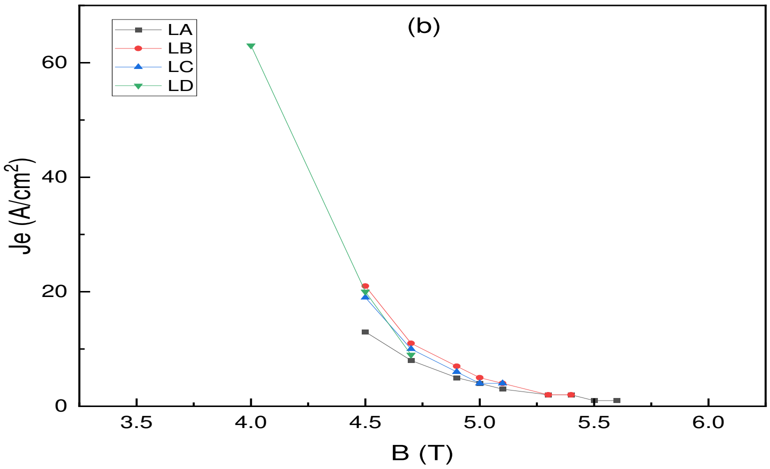
(b)
LA
LB
LC
LD
Je (A/cm^2)
B (T)

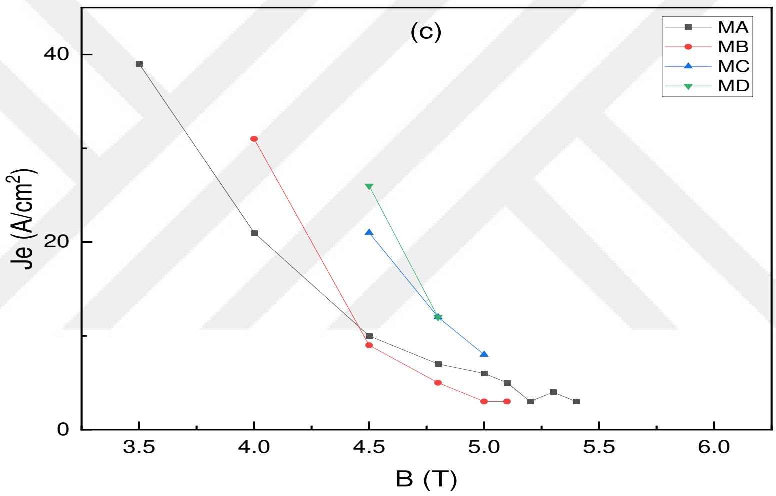
(c)
MA
MB
MC
MD
Je (A/cm^2)
B (T)

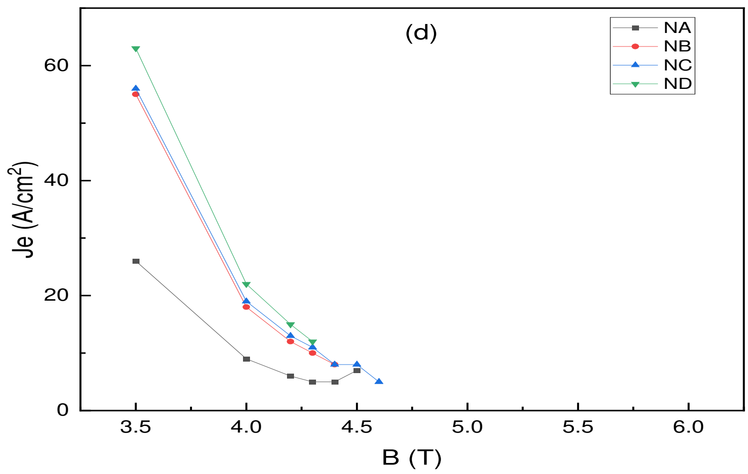
(d)
NA
NB
NC
ND
Je (A/cm^2)
B (T)

Figure 6.13. J_e vs. B curves for tapes samples, a) KA, KB, and KC of 1.2 mm thickness, b) LA, LB, LC, and LD of 0.9 mm thickness, c) MA, MB, MC, and MD of 0.6 mm thickness, d) NA, NB, NC, and ND of 0.4 mm thickness.

Our results did not align with our expectations regarding the effects of wire diameter and progressive flat rolling wires and tapes. As the wire diameters and tape thicknesses decreased, the critical current values worsened, which is contrary to what we would anticipate.

There may various reasons for these observations. These reasons may be related to the behaviour of the superconducting samples at different temperatures while carrying different currents under different magnetic fields. They may be due to differences occurring during mechanical processing steps and during chemical reaction for phase formation and sintering.

First of all, the critical current (I_c) values measured at higher temperatures using a current as small as 1 ampere do not provide a definitive understanding of the samples' behavior. As the temperature decreases, differences in critical current values may favour thinner samples. Without conducting tests, we cannot be certain. Additionally, in our laboratories, we lack the necessary equipment to measure larger currents at cryogenic temperatures.

The mesh size of the Mg powder we utilized is 100 mesh, indicating it is not a fine powder. Handling very fine magnesium powders in an open atmosphere is not feasible; it requires a glovebox medium under an inert gas, such as argon. Although we could have used 325 mesh Mg powder for the initial Mg+2B powder mixture, we opted not to at the beginning.

Another approach to mitigate this issue would involve employing a longer high-energy ball milling process to more efficiently mix the Mg and B powders until their particle size is significantly reduced. This process also necessitates an inert gas atmosphere, where the powder should be filled into iron tubes inside a glovebox, with both ends sealed.

During the process of flat rolling for tape production, the tape's width increases. This, in turn, lengthens the required diffusion distance for Mg atoms to travel and participate in the reactive formation of MgB_2 with B atoms. These factors potentially contribute to the compromised properties of the tapes when they undergo additional flat rolling.

Flat rolling also leads to increased density of the inner ceramic core in the tapes, thereby slowing down the diffusion of Mg atoms (Mg vapor). Consequently, longer heat treatment durations may be required for tapes compared to wires. However, there is a limit to this, as excessive heat treatment can result in undesired reactions between the MgB_2 core material and the iron sheath.

7. CONCLUSIONS

Our aim was to produce wires of different diameters and tapes of different thicknesses to obtain the best superconducting properties in these samples. Thicker wires elongated more, and thinner wires elongated less upon flat rolling. Therefore, the wires suffer less deformation than the tapes. As a result of the cryogenic tests and analyzes, the samples with the higher critical temperature T_c and engineering critical current density J_e among the samples were identified. However, in group A, the wire sample with a diameter of 2.5mm recorded the highest T_c at 37.71K. Whereas the tape sample with a thickness of 0.6mm recorded the lowest normal state resistivity at 68 μΩ.cm among all the samples measured. The same sample recorded the highest J_e value of 39 A/cm^2 at 3.5T magnetic field. In group B, which includes a wire with a diameter of 2.0 mm and tapes of different thicknesses, the tape sample with a thickness of 1.2mm recorded the highest T_c at 37.76K and the lowest normal state resistivity at 131μΩ.cm. In contrast, the tape sample with a thickness of 0.4mm recorded the highest J_e value of 55 A/cm^2 under 3.5T magnetic field. In group C, the wire sample with a diameter of 1.7 mm recorded the highest T_c at 37.87 K among the samples of this group and among all the samples measured, and the tape sample with a thickness of 1.2mm also recorded the lowest normal state resistivity at 105 μΩ.cm. In contrast, the tape sample with a thickness of 0.4mm recorded the highest J_e value of 56A/cm^2 at 3.5T magnetic field. In group D, the wire sample with a diameter of 1.3mm recorded the highest T_c at 37.73K, while the tape sample with a thickness of 0.9mm recorded the lowest normal state resistivity at 152μΩ.cm. Whereas the tape samples with a thickness of 0.9mm and 0.4mm recorded the highest J_e value of 63A/cm^2 at 4T and 3.5T magnetic field. Thus, the results showed that the critical engineering current density J_e behaviours with the magnetic field. Therefore, samples with larger dimensions, wire diameter or tape thickness tend to have higher J_e values. Tapes of smaller thickness show faster degradation of J_e, which makes them less suitable for applications involving strong magnetic fields.

As a result, through this study, we conclude that the wires and tapes, the greater their cross-sectional area, the greater their ability to withstand higher magnetic fields, in addition to having higher J_e and T_c values. This phenomena may be related to the diffusion of magnesium during sintering heat treatment process. Although the transport super current-carrying capacity of these tapes tends to decrease when made thinner, it can still be advantageous when employing the react and wind technique for coil winding. Thinner tapes are able to endure higher bending strains with a lesser reduction in their critical current values caused by bending.

8. REFERENCES

Vancouver citation style was used in this thesis.

1. Onnes HK. Further experiments with liquid helium. H. On the electrical resistance of pure metals etc. VII. The potential difference necessary for the electric current through mercury below 4°.19 K. InKNAW, Proc. 1913;15:1406–30.

2. Zhou S, Zhang Y, Pan A V., Dou SX, Chung KC, Kim YK, et al. Effects of sintering atmosphere on the superconductivity of MgB2. Supercond Sci Technol. 2009;22(4).

3. Ford PJ SG. The rise of the superconductors. CRC Press. 2004;

4. Buzea C YT. Review of the superconducting properties of MgB2. Supercond Sci Technol. 2001;14(11):R115.

5. Collings EW, Sumption MD, Bhatia M, Susner MA, Bohnenstiehl SD. Prospects for improving the intrinsic and extrinsic properties of magnesium diboride superconducting strands. Supercond Sci Technol. 2008;21(10).

6. Yamamoto A, Shimoyama JI, Kishio K, Matsushita T. Limiting factors of normal-state conductivity in superconducting MgB 2: An application of mean-field theory for a site percolation problem. Supercond Sci Technol. 2007;20(7):658–66.

7. Serquis A, Civale L, Hammon DL, Liao XZ, Coulter JY, Zhu YT, et al. Hot isostatic pressing of powder in tube MgB2 wires. Appl Phys Lett. 2003;82(17):2847–9.

8. Gajda D, Morawski A, Zaleski A, Kurnatowska M, Cetner T, Gajda G, et al. The influence of HIP on the homogeneity, Jc, Birr, Tc and Fp in MgB2 wires. Supercond Sci Technol. 2014;28(1).

9. Cetner T, Morawski A, Adamczyk K, Rindfleisch M, Tomsic M, Zaleski A, et al. Improvement of critical properties of undoped, multifilamentary MgB2 wires in Nb/Cu after annealing under high gas pressure. High Press Res. 2012;32(3):419–24.

10. Giunchi G, Ceresara S, Ripamonti G, Di Zenobio A, Rossi S, Chiarelli S, et al. High performance new MgB2 superconducting hollow wires. Supercond Sci Technol. 2003;16(2):285–91.

11. Hur JM, Togano K, Matsumoto A, Kumakura H, Wada H, Kimura K. Fabrication of high-performance MgB2 wires by an internal Mg diffusion process. Supercond Sci Technol. 2008;21(3):2–6.

12. Jie H, Qiu W, Billah M, Mustapic M, Patel D, Ma Z, et al. Superior transport Jc obtained in in-situ MgB2 wires by tailoring the starting materials and using a combined cold high pressure densification and hot isostatic pressure treatment. Scr Mater. 2017;129:79–83.

13. Maeda M, Hossain MS Al, Motaman A, Kim JH, Kario A, Rindfleisch M, et al. Synergetic combination of LIMD with CHPD for the production of economical and high performance MgB2 Wires. IEEE Trans Appl Supercond. 2013;23(3):9–12.

14. Gao Z, Wang D, Zhang X, Ma Y, Awaji S, Nishijima G, et al. Simultaneous introduction of scattering and pinning in organic rare-earth salt doped MgB2 tapes. Supercond Sci Technol. 2010;23(4).

15. Yang F, Li SQ, Yan G, Feng JQ, Xiong XM, Zhang SN, et al. Improved superconducting properties in Ti-doped MgB2 prepared by two-step reaction method and high-energy ball milling. J Alloys Compd. 2015;622:714–8.

16. Kim JH, Zhou S, Hossain MSA, Pan A V., Dou SX. Carbohydrate doping to enhance electromagnetic properties of MgB 2 superconductors. Appl Phys Lett. 2006;89(14).

17. Zeng R, Lu L, Wang JL, Horvat J, Li WX, Shi DQ, et al. Significant improvement in the critical current density of in situ MgB 2 by excess Mg addition. Supercond Sci Technol. 2007;20(8):0–5.

18. Susner MA, Sumption MD, Bhatia M, Peng X, Tomsic MJ, Rindfleisch MA, et al. Influence of Mg/B ratio and SiC doping on microstructure and high field transport Jc in MgB2 strands. Phys C Supercond. 2007;456(1–2):180–7.

19. Matsumoto A, Kumakura H, Kitaguchi H, Senkowicz BJ, Jewell MC, Hellstrom EE, et al. Evaluation of connectivity, flux pinning, and upper critical field contributions to the critical current density of bulk pure and SiC-alloyed MgB 2. Appl Phys Lett. 2006;89(13):1–2.

20. Klie RF, Idrobo JC, Browning ND, Regan KA, Rogado NS, Cava RJ. Direct observation of nanometer-scale Mg- and B-oxide phases at grain boundaries in MgB2. Appl Phys Lett. 2001;79(12):1837–9.

21. Zhang H, Zhao Y, Zhang Y. The Effects of Excess Mg Addition on the Superconductivity of MgB2. J Supercond Nov Magn. 2015;28(9):2711–4.

22. Chen SK, Serquis A, Serrano G, Yates KA, Blamire MG, Guthrie D, et al. Structural and superconducting property variations with nominal Mg non-stoichiometry in MgxB2 and its enhancement of upper critical field. Adv Funct Mater. 2008;18(1):113–20.

23. Li XH, Du XJ, Qiu M, Ma YW, Xiao LY. Design and experimental demonstration of an MgB2 based 1.5 T MRI test magnet. Phys C Supercond its Appl. 2007;463–465(SUPPL.):1338–41.

24. Karaboğa F, Yetiş H, Akdoğan M, Belenli İ. Monofilamentary In Situ Fe/MgB2 Superconducting Wires Fabricated by Pellet-in-Tube Method. J Supercond Nov Magn. 2018;31(5):1359–67.

25. Q W. Fabrication and superconducting properties of MgB2/Nb/Cu wires with chemical doping by using Powder-In-Tube (PIT) method. Univ Joseph-Fourier-Grenoble I. 2014;

26. Wolfbrandt A, Magnusson N. AC losses in high-temperature superconducting tapes exposed to perpendicular magnetic fields combined with transport currents. Supercond Sci Technol. 2002;15(4):572–6.

27. Maeda H, Tanaka Y, Fukutomi M, Asano T. A new High-Tc oxide superconductor without a rare earth element. Jpn J Appl Phys. 1988;27(2A):L209–10.

28. Wu MK, Ashburn JR, Torng CJ, Hor PH, Meng RL, Gao L, et al. Superconductivity at 93 K in a new mixed-phase Yb-Ba-Cu-O compound system at ambient pressure. Phys Rev Lett. 1987;58(9):908–10.

29. Rautiainen K, Kainulainen J, Auer T, Tauriainen S, Hallikainen M. Helsinki University of Technology L-band airborne synthetic aperture radiometer. IEEE Trans Geosci Remote Sens. 2008;46(3):717–26.

30. Meissner W, Ochsenfeld R. Ein neuer effekt bei eintritt der supraleitfähigkeit. Naturwissenschaften. 1933;21(44):787–8.

31. A M. Room-temperature superconductivity. Cambridge Int Science Publishing. 2004.

32. Sharma RG. Superconductivity: Basics and applications to magnets. Springer Nature. 2021.

33. Bardeen J, Cooper LN SJ. Theory of superconductivity. Phys Rev. 1957;108(5):1175.

34. London F LH. The electromagnetic equations of the supraconductor. Proc R Soc London Ser A-Mathematical Phys Sci. 1935;149(866):71–88.

35. Ginzburg VL. On the theory of superconductivity. Nuovo Cim Ser 10. 1955;2(6):1234–50.

36. Zhao Y, Huang DX, Feng Y, Cheng CH, MacHi T, Koshizuka N, et al. Nanoparticle structure of MgB2 with ultrathin TiB2 grain boundaries. Appl Phys Lett. 2002;80(9):1640–2.

37. Abrikosov AA. On the Magnetic Properties of Superconductors of the Second Group. Sov Phys Jetp. 1957;5(6):1174–82.

38. Sumption MD, Bhatia M, Rindfleisch M, Phillips J, Tomsic M CE. MgB2/Cu racetrack coil: winding and transport Testing. arXiv Prepr cond-mat/0410450. 2004;1–20.

39. Bednorz JG MK. Possible high Tc superconductivity in the Ba− La− Cu− O system. Zeitschrift für Phys B Condens Matter. 1986;64(2):189–93.

40. Josephson BD. Possible new effects in superconductive tunnelling. Phys Lett. 1962;1(7):251–3.

41. Cantoni M, Schilling A, Nissen HU, Ott HR. Characterisation of superconducting Hg-Ba-Ca-Cu-oxides: Structural and physical aspects. Phys C Supercond. 1993;215(1–2):11–8.

42. Dai P, Chakoumakos BC, Sun GF, Wong KW, Xin Y, Lu DF. Synthesis and neutron powder diffraction study of the superconductor HgBa2Ca2Cu3O8 + δ by Tl substitution. Phys C Supercond. 1995;243(3–4):201–6.

43. Jones ME, Marsh RE. The Preparation and Structure of Magnesium Boride, MgB2. J Am Chem Soc. 1954;76(5):1434–6.

44. Yildirim T, Gülseren O, Lynn JW, Brown CM, Udovic TJ, Huang Q, et al. Giant anharmonicity and nonlinear electron-phonon coupling in MgB2: A combined first-principles calculation and neutron scattering study. Phys Rev Lett. 2001;87(3):37001-1-37001–4.

45. Osborn R, Goremychkin EA, Kolesnikov AI, Hinks DG. Phonon density of states in MgB2. Phys Rev Lett. 2001;87(1):3–6.

46. Yildirim T, Gülseren O. A simple theory of 40 K superconductivity in MgB2: First-principles calculations of Tc, its dependence on boron mass and pressure. J Phys Chem Solids. 2002;63(12):2201–6.

47. Cardwell DA, Ginley DS E. Handbook of superconducting materials. Crc Press. 2003;1.

48. Tomsic M, Rindfleisch M, Yue J, McFadden K, Doll D, Phillips J, et al. Development of magnesium diboride (MgB2) wires and magnets using in situ strand fabrication method. Phys C Supercond. 2007;456(1–2):203–8.

49. Bhagurkar AG, Yamamoto A, Babu NH, Durrell JH, Dennis AR, Cardwell DA. Synthesis of dense bulk MgB2 by an infiltration and growth process. Supercond Sci Technol. 2014;28(1).

50. Bud'ko SL, Petrovic C, Lapertot G, Cunningham CE, Canfield PC, Jung MH, et al. Magnetoresistivity and Hc2(T) in MgB2. Phys Rev B. 2001;63(22):220503.

51. Ulgen AT, Belenli I. The Effect of Fe Diffusion on Some Physical and Superconducting Properties of MgB2. J Supercond Nov Magn. 2017;30(4):1089–95.

52. Tanaka K, Kitaguchi H, Kumakura H, Hirakawa M, Yamada H OM. Fabrication and

transport properties of MgB2 mono-core wire and solenoid coil. IEEE Trans Appl Supercond. 2005;15(2):3180–3.

53. Glowacki BA, Majoros M, Vickers M, Evetts JE, Shi Y MI. Superconductivity of powder-in-tube MgB2 wires. Supercond Sci Technol. 2001;14(4):193.

54. M Y. Fabrication and Characterization of MgB2 Powders and Cu-Clad MgB2 Wires. Izmir Inst Technol. 2005;

55. Matsumoto A, Kumakura H, Kitaguchi H, Fujii H, Togano K. The annealing effects of MgB2 superconducting tapes. Phys C Supercond. 2002;382(2–3):207–12.

56. Jin S, Mavoori H VDR. High transport critical currents in dense, metal-clad superconductor wires of MgB2. arXiv Prepr cond-mat/0104236. 2001;1–12.

57. Kitaguchi H, Kumakura H TK. Strain effect in MgB2/stainless steel superconducting tape. Phys C Supercond. 2001;363(3):198–201.

58. Feng Y, Zhao Y, Pradhan AK, Zhou L, Zhang PX, Liu XH, Ji P, Du SJ, Liu CF, Wu Y KN. Fabrication and superconducting properties of MgB2 composite wiresby the PIT method. Supercond Sci Technol. 2001;15(1):12.

59. Li WX, Li Y, Zhu MY, Chen RH, Dou SX, Qin MJ, Xu X YP. Effect of magnetic field processing on the microstructure of micronsize Zn doped MgB2. Phys C Supercond its Appl. 2007;460:310–1.

60. Sumption MD, Bhatia M, Dou SX, Rindfliesch M, Tomsic M, Arda L, Ozdemir M, Hascicek Y CE. Irreversibility field and flux pinning in MgB2 with and without SiC additions. Supercond Sci Technol. 2004;17(10):1180.

61. Giunchi G, Orecchia C, Malpezzi LU MN. Analysis of the minority crystalline phases in bulk superconducting MgB2 obtained by reactive liquid Mg infiltration. Phys C Supercond its Appl. 2006;433(3–4):182–8.

62. Wang QY, Jiao GF, Liu GQ, Xiong XM, Yan SC, Zhang PX, Sulpice A, Mossang E, Feng Y YG. Fabrication and properties of multifilamentary MgB2 wires by in-situ powder-in-tube process. Phys C Supercond its Appl [Internet]. 2010;470(20):1415–8. Available from: http://dx.doi.org/10.1016/j.physc.2010.05.126

63. Shan D, Yan G, Zhou L, Wang Q, Xiong X, Jiao G, et al. Effect of Ti3SiC2 doping on critical current density and flux pinning in MgB2. Cryogenics (Guildf) [Internet]. 2012;52(10):482–5. Available from: http://dx.doi.org/10.1016/j.cryogenics.2012.05.013

64. Fu BQ, Feng Y, Yan G, Zhao Y, Pradhan AK, Cheng CH, et al. High critical current density in Ti-doped MgB2/Ta/Cu tape by powder-in-tube process. J Appl Phys. 2002;92(12):7341–4.

65. Kumakura H, Matsumoto A, Fujii H, Togano K. High transport critical current density obtained for powder-in-tube-processed MgB2 tapes and wires using stainless steel and Cu-Ni tubes. Appl Phys Lett. 2001;79(15):2435–7.

66. Goldacker W, Schlachter SI, Zimmer S, Reiner H. High transport currents in mechanically reinforced MgB2 wires. Supercond Sci Technol. 2001;14(9):787–93.

67. Song KJ, Lee NJ, Jang HM, Ha HS, Ha DW, Oh SS, Sohn MH, Ko RK, Park C, Kwon YK RK. Single-filament composite MgB2/stainless-steel ribbons by powder-in-tube process. Phys C Supercond. 2002;370(1):21–6.

68. Mizuno K, Uchiyama D, Maeda M, Akao T, Kawakami T, Kubota Y, et al. Microstructure and critical current densities of MgB2/Cu wires. IEEE Trans Appl Supercond.

2005;15(2):3345–8.

69. Nakane T, Takahashi K, Kitaguchi H, Kumakura H. Fabrication of Cu-sheathed MgB2 wire with high Jc-B performance using a mixture of in situ and ex situ PIT techniques. Phys C Supercond its Appl [Internet]. 2009;469(15–20):1531–5. Available from: http://dx.doi.org/10.1016/j.physc.2009.05.227

70. Strickland NM, Buckley RG, Otto A. Enhanced critical current densities in Cu-sheathed MgB2. Curr Appl Phys. 2004;4(6):688–92.

71. Fang H, Gijavanekar P, Zhou YX, Putman PT, Salama K. Development of Fe-sheathed MgB2 wires and tapes for electric power applications. IEEE Trans Appl Supercond. 2005;15(2):3200–3.

72. Wang D, Ma Y, Yu Z, Gao Z, Zhang X, Watanabe K, et al. Strong influence of precursor powder on the critical current density of Fe-sheathed MgB2 tapes. Supercond Sci Technol. 2007;20(6):574–8.

73. Tachikawa K, Yamada Y, Katagiri K, Kumakura H, Iwamoto A WK. Effects of Metal Powder Addition in Ni-Sheathed PIT MgB2 Tapes. Ina Conf Proc. 2004;711(1):561–8.

74. Beilin V, Felner I, Tsindlekht MI, Dul'kin E, Mojaev E, Roth M. Critical state instability in Nb-clad MgB2 superconducting wires. Phys C Supercond its Appl. 2008;468(3):223–8.

75. Kováč P, Hušek I, Melišek T, Kulich M, Štrbík V. MgB2 composite wires with Fe, Nb and Ta sheaths. Supercond Sci Technol. 2006;19(6):600–5.

76. Song KJ, Kim SW, Park C, Joo JH, Choi SJ, Ko RK, et al. The effect of geometry of composite MgB2/stainless-steel (SS) wires fabricated by PIT process on the superconducting properties. Phys C Supercond its Appl. 2004;407(1–2):17–22.

77. Tobin JR. Superconductivity Research Developments. Nova Publishers. 2008.

78. Ma ZQ, Liu YC. Low-temperature synthesis of MgB2 superconductors. Int Mater Rev. 2011;56(5–6):267–86.

79. Lee S. Crystal growth of MgB2. Phys C Supercond. 2003;385(1–2):31–41.

80. Serquis A, Civale L, Hammon DL, Coulter JY, Liao XZ, Zhu YT, et al. Microstructure and high critical current of powder-in-tube MgB2. Appl Phys Lett. 2003;82(11):1754–6.

81. Yamamoto A, Shimoyama JI, Ueda S, Katsura Y, Horii S, Kishio K. Improved critical current properties observed in MgB2 bulks synthesized by low-temperature solid-state reaction. Supercond Sci Technol. 2004;18(1):116–21.

82. Chen SK, Tan KS, Glowacki BA, Yeoh WK, Soltanian S, Horvat J, et al. Effect of heating rates on superconducting properties of pure MgB2, carbon nanotube- and nano-SiC-doped in situ MgB2 Fe wires. Appl Phys Lett. 2005;87(18):1–3.

83. Zhao Q, Liu Y, Han Y, Ma Z, Shi Q, Gao Z. Effect of heating rates on microstructure and superconducting properties of pure MgB2. Phys C Supercond its Appl [Internet]. 2009;469(14):857–61. Available from: http://dx.doi.org/10.1016/j.physc.2009.06.002

84. Chen SK, Wei M, MacManus-Driscoll JL. Strong pinning enhancement in MgB2 using very small Dy 2O3 additions. Appl Phys Lett. 2006;88(19):1–13.

85. Shcherbakova O V., Pan A V., Soltanian S, Dou SX. Cooling rate effect on microstructure and superconducting properties of pure and SiC doped MgB2 superconductors. Phys C Supercond its Appl. 2007;460:579–80.

86. Dou SX, Horvat J, Soltanian S, Wang XL, Qin MJ, Zhou SH, et al. Transport critical current density in Fe-sheathed nano-SiC doped MgB2 wires. IEEE Trans Appl Supercond. 2003;13(2):3199–202.

87. Sawada M, Shimoyama J ichi, Takagi N, Motoki T, Kodama M, Tanaka H. A new carbon source MgB2C2 for the synthesis of carbon-doped MgB2 materials. Solid State Commun. 2018;281:53–6.